The Impact of Oceanic Feedbacks on Stratosphere-Troposphere Coupling in an Idealised Model

N. E. Trencham[1], A. Czaja[1], and J. D. Haigh[1,2]

[1]Department of Physics, Imperial College London, London, UK, [2]Grantham Institute on Climate Change and the Environment, Imperial College London, London, UK

Corresponding author: N. Trencham (net2130@columbia.edu)

Key Points:

- Ocean feedbacks significantly alter the atmospheric response to applied stratospheric temperature perturbations after 100-200+ years;
- Changes in low-latitude ocean heat content, driven by changes in Ekman transport, are responsible.

Abstract

Stratospheric temperature perturbations (STPs) caused by e.g. variations in stratospheric ozone, are an important driver of changes in tropospheric dynamics, particularly pertinent to the long-term climate evolution of the Southern Hemisphere. However, the impact of ocean feedbacks on this interaction has not been fully examined. To study it, positive STPs were applied in three otherwise identical, idealised model configurations –atmosphere-only (A), atmosphere + slab-ocean (AS), and fully-coupled atmosphere-ocean (AO) – and the resulting atmospheric changes compared. In the AO model, changes in the tropics/extratropics experienced a positive/negative feedback after ~100-200 years, whilst the AS model showed few significant changes, compared to the A model. Changes in tropical ocean heat content were responsible, attributable to changes in the Ekman transport. These results indicate that full atmosphere-ocean coupling should be accounted for when studying the long-term (100+ years) tropospheric response to STPs in the Southern Ocean region. Validation with higher-resolution and more realistic models is necessary.

Plain Language Summary

In recent decades, the Southern Ocean region has seen significant climatic changes in response to stratospheric ozone depletion. It is important to understand what impact oceanic feedbacks might have on this response. To that end, experiments were performed, in which temperature perturbations were applied to the stratospheres of three otherwise identical atmospheric models – with/without oceans present – and their results compared. Ocean feedbacks were found to significantly amplify/weaken and expand/shift the atmospheric responses towards the poles in the tropics/extratropics after about 100-200 years. This was caused by wind-driven changes in sea surface temperatures at low-latitudes. These results underscore the importance of accounting for oceanic feedbacks when studying long-term (100+ years) climatic changes, caused by stratospheric changes, in the Southern Ocean region. However, further verification of these results with higher-resolution and more realistic models will be necessary to ensure their applicability, and to better quantify their effects.

1 Introduction

As the region containing over 90% of atmospheric ozone - a strong absorber of UV radiation, and an important greenhouse gas - the stratosphere is of huge importance to Earth's radiative balance. Furthermore, in the late 90s/2000s, numerous studies demonstrated a downward dynamical influence of stratospheric zonal wind and/or temperature perturbations upon the tropospheric below (e.g. Baldwin & Dunkerton 1999; Polvani & Kushner 2002; Kushner & Polvani 2004; Haigh et al. 2005; Lorenz & DeWeaver 2007; Simpson et al. 2009). Since ozone concentrations can influence stratospheric temperatures, they can also – via thermal wind balance – influence stratospheric zonal winds. Thus, fluctuations in the levels of stratospheric ozone, and other chemical species, have the potential to influence the troposphere both radiatively and – though their influence upon stratospheric temperatures and zonal winds - dynamically.

More recently, studies examining the impact of 20th century changes in stratospheric ozone in the Southern Hemisphere found them to be responsible for most of the observed climatic changes over that timeperiod, with decreases in polar stratospheric ozone causing cooling, inducing a poleward-shift in the tropospheric zonal winds and circulations (Polvani et al. 2011; Son et al. 2018; see Chapter 4 of Karpechko et al. (2019) for an overview). Looking ahead, the recovery in stratospheric ozone has the potential to mitigate, or even cancel out, further climatic changes which are driven by increasing levels of greenhouse gases (Gerber & Son 2014).

Further, numerous studies have simulated an oceanic response to varying levels of stratospheric ozone in the Southern Hemisphere, and the changes in surface wind stress they produce (Cai 2006; Cai & Cowen 2007; Wang et al. 2014; Ferreira et al. 2015; Seviour et al. 2016). These studies found that, accompanying the poleward shift in the tropospheric midlatitude jet, an enhanced midlatitude ocean circulation was produced, causing an increased poleward heat transport into the midlatitudes, and anomalous vertical upwelling at higher latitudes. The net result was an increase in midlatitude sea surface temperatures (SSTs), and an initial decrease (~0-20/25 years) followed by a long-term increase (20/25+ years) in SSTs poleward.

It is therefore clear that varying levels of stratospheric ozone can exert a profound influence over both the troposphere and ocean, especially in the Southern Hemisphere. However, relatively few of the studies which simulated this type of stratosphere-troposphere coupling with fully coupled atmosphere-ocean models (e.g. Ferreira et al. 2015) have examined the interaction between these different couplings, and whether the presence of a fully dynamical ocean might have an impact. Sigmond et al. (2010) found no discernable impact of atmosphere-ocean coupling upon the tropospheric response to ozone depletion. Neither did other studies, concerned with the robustness of the tropospheric response to ozone depletion across different models (Seviour et al. 2017; Son et al. 2018). Some of these were fully-coupled, but they generally suffered from a relatively short timeperiod of study (max 100 years), and large model internal variability, compounded by a small (often one) ensemble size, obscuring the significance of any impact.

That said, there have been some studies looking at the oceanic response to solar variability and stratospheric extratropical variability, and feedbacks upon the atmosphere, mainly in the Northern Hemisphere. For example, Reichler et al. (2012) and Menary & Scaife (2014) found evidence of decadal-scale changes in Atlantic Meridional Overturning Circulation

(AMOC) strength in response to successive strong polar vortex events and solar variability respectively. O'Callaghan et al. (2014) also found evidence of implied surface heat flux anomalies in the North Atlantic, in response to SSW events. Simulations and analyses performed by Scaife et al. (2013) and Andrews et al. (2015) found evidence of a lagged amplification of solar cycle-induced anomalies in the North Atlantic Oscillation (NAO), mediated via NAO-induced SST anomalies in the North Atlantic. Omrani et al. (2014) also found evidence of downward-propagating negative NAO stratospheric anomalies during boreal winter, in response to decadal-scale North Atlantic SST anomalies. This all serves to suggest that solar and extratropical stratospheric variability plays a role in the forcing of North Atlantic oceanic variability, which can in turn feed back onto the troposphere and stratosphere via altered SSTs.

Here we examine the impact of atmosphere-ocean coupling on the tropospheric response to imposed stratospheric temperature perturbations (STPs) by imposing them in three different global atmosphere model configurations – atmosphere-only (A), atmosphere and slab-ocean (AS), and fully-coupled atmosphere and ocean (AO) – and comparing the responses. Section 2 provides an outline of the model, configurations and equations used, and experiments performed. Section 3 details the results of these experiments, and mechanisms involved. Section 4 discusses these results, their limitations, and the conclusions and broader implications of this study.

2 Methodology

2.1 Model setup and experiments

Simulations were carried out with the MITgcm model, placed in an aquaplanet, double-drake (two oceanic ridges, 90ºN to 30ºS, 90º longitudinal separation; see Ferreira et al. (2015) for more details) configuration, with no seasonal or diurnal cycle. This model utilises the full set of atmospheric and oceanic hydrodynamic equations via a single dynamical core, and parameterisations of various sub-gridscale physical processes, such as diffusion and convection, which follow O'Gorman & Schneider (2008). A two-stream gray radiation package (see supporting information of Geen et al. 2016) was used, and no representations of ice or clouds were included. Albedo was held fixed at 37%.

For each of the three configurations (A, AS and AO), the model used a 192x32 cube-sphere grid, with an approximate horizontal resolution of 3º-4º, and 25 evenly spaced atmospheric pressure levels, 980 to 20hPa. Although the low vertical resolution (3-7 levels) and low-top in the model stratosphere will mean a full representation of stratospheric dynamics is not possible, this is arguably not necessary when studying the impact of imposed temperature perturbations in the lower stratosphere upon the troposphere below. This is because the primary mechanism of this downwards impact involves stratospheric control of upward-propagating planetary and synoptic-scale waves, mediated by changes in the quasigeostrophic potential vorticity gradient (QG PV gradient), which peaks around the lower stratosphere/upper troposphere. (Simpson et al. 2009; White et al. 2020)

In the AO model, the ocean has 15 vertical levels, 0-3400m, with increasing vertical spacing from top to bottom (table S1). In the AS model, the ocean is a non-dynamical 'slab' of fixed depth 50m, with heat transport parameterised as a constant 'Q-flux' term. The A model is

identical to the AS model, except that its SSTs are held fixed. The model atmosphere was the same across each configuration.

Model version	Atmosphere/Ocean dynamics	Equilibration time (approximate)	Ensemble Size	Experiments performed	Experiments duration (after equilibration of initial state)
AO	Full atmospheric dynamics Full ocean dynamics	2000 years	8	U0 (control), U01, P01, T01	300 years
AS	Full atmospheric dynamics Slab-ocean	10 years	6	U0 (control), U01, P01, T01	50 years
A	Full atmospheric dynamics Fixed SSTs	200 days	6	U0 (control), U01, P01, T01 SST perturbation experiments	30 years

Table 1: Summary of the different model versions used, their representations of atmospheric and oceanic dynamics, equilibration times, experiments performed, their durations, and ensemble sizes.

To set up the model control states, the following steps were performed. The AO model was run until equilibrium (considered a global-average net surface heat flux of magnitude $<0.1 \mathrm{Wm}^{-2}$). Its SSTs (figure S1) and net ocean heat fluxes (figure S2) were then diagnosed, and applied to the simplified oceans of the A and AS models, as the SST and Q-flux values respectively.

For each model version, different ensemble member initial states were constructed, for use in subsequent experiments. For the AO model, these were obtained by taking eight separate snapshots of the equilibrated control simulation at 10-year intervals. For the AS and A models, these were obtained by applying six different temperature and humidity profiles to the model atmospheres and allowing the models to run to equilibrium.

Once the equilibrated ensemble member initial states had been obtained, each was used to perform four separate simulations: one control, and three experiments (U01, P01, & T01). In the experimental runs, STPs were applied via the addition of a constant warming rate of +0.1ºC/day to the radiative temperature tendency. These were applied in the stratosphere only, diagnosed as the atmospheric region in which the lapse rate falls and remains below 2°C/km (figure S3). The STPs were applied over the entire stratosphere (U01), or regions of finite latitudinal extent in both hemispheres: 30°S to 30°N (T01), and 60° to 90°S/N (P01). These STPs were designed to

produce temperature signals in the lower stratosphere which qualitatively resembled those caused by e.g. ozone depletion/recovery (P01), or 11-year solar cycle variability (T01), whilst also being quantitatively of the same order of magnitude. Each control and experimental ensemble simulation was run for 30/50/300 years in the A/AS/AO model. See table 1 for a summary of the experiments, their durations and ensemble sizes, in each model version. Since the response of U01 in the A model resembled a weakened version of P01 (see figure S4), we will mostly omit this experiment from our results.

By comparing between the simulations with and without the STPs present, their effect on the model atmospheres and oceans may be ascertained. Moreover, comparison of the atmospheric anomalies obtained in response to the same STPs, applied across different (A vs. AS/AO) model versions, can elucidate the impact of atmosphere-ocean coupling upon this interaction. In contrast to previous studies (e.g. Sigmond et al. 2010), by utilising relatively long model runs and large ensemble sizes, the obscuring effects of internal model variability should be minimised.

To isolate the role of SST anomalies in altering the atmospheric response to applied STPs, separate SST-perturbation experiments were also performed. In these, SST perturbations – derived all or in part from the SST anomalies obtained in response to experiments P01 and T01 in the AO model (figures 4, S9) – were applied in the A model. These were applied for 5 years to each previously detailed ensemble member, and compared to corresponding control runs. In addition, to investigate how the atmospheric response to SST perturbations was initiated, the SST anomaly found in U01 in the AS model (figure 4, green curve) was applied for 36 days in the A model, with an ensemble size of 24, and compared to a control run of identical ensemble size and duration.

2.2 Dynamical diagnostics

To understand better the mechanisms behind the atmospheric and oceanic response to SST changes and STPs respectively, various atmospheric and oceanic equations will be utilised in section 3.4. For the atmosphere, we utilise the Transformed Eulerian Mean (TEM) meridional velocity, $\tilde{v}$, and streamfunction, $\tilde{\psi}$, as developed by Andrews & McIntyre (1976):

$$\tilde{v} = v - \frac{\partial}{\partial p}\left(\frac{\overline{v'\theta'}}{\partial_p \theta}\right) \tag{1}$$

$$\tilde{\psi} = \frac{2\pi R \cos\varphi}{g}\int_{p_0}^{p} \tilde{v}\,dp' = \psi - \frac{\overline{v'\theta'}}{\partial_p \theta} \tag{2}$$

where v and ψ is the Eulerian meridional velocity and mass streamfunction respectively, p is pressure, θ is the potential temperature, R is Earth's radius, φ is the latitude in radians, and v' indicates a deviation of v from the zonal mean. This formulation reduces the zonal-mean zonal velocity, u, equation to:

$$\frac{\partial u}{\partial t} = f\tilde{v} + F_x + \frac{1}{R\cos\varphi}\boldsymbol{\nabla}.\mathbf{F} \tag{3}$$

where t is time, f is the Coriolis parameter, F_x is the zonal friction component, and $\boldsymbol{\nabla}.\mathbf{F}$ Is the Eliassen-Palm (EP) flux divergence (see e.g. Peixoto & Oort 1992). For the purposes of constructing EP flux diagrams, we will follow Edmon et al. (1980), and use annular mass-weighted versions of the EP fluxes, $\tilde{\mathbf{F}} = \left(\tilde{\mathrm{F}}_y, \tilde{\mathrm{F}}_p\right)$:

$$\tilde{\mathrm{F}}_\varphi = \frac{2\pi R}{g}\mathrm{F}_\varphi = -\frac{2\pi R^2\cos^2\varphi}{g}\overline{u'v'} \tag{4}$$

$$\tilde{\mathrm{F}}_p = \frac{2\pi R^2\cos\varphi}{g}\mathrm{F}_y = -\frac{2\pi R^3 f\cos^2\varphi}{g\partial_p\theta}\overline{v'\theta'} \tag{5}$$

Following quasigeostrophic (QG) theory, the EP flux divergence is equal to the poleward eddy flux of potential vorticity (PV, q), $\overline{v'q'}$ (e.g. Vallis 2006). If these fluxes are downgradient, we would therefore expect a net EP flux convergence/divergence towards/away from regions of positive/negative meridional PV gradient, given under QG theory as:

$$q_\varphi = 2\Omega\cos\varphi - \frac{\partial}{\partial\varphi}\left(\frac{\partial_\varphi(u\cos\varphi)}{R\cos\varphi}\right) + \frac{f^2R}{R_d}\frac{\partial}{\partial p}\left(\frac{p\theta}{T}\frac{\partial_p u}{\partial_p\theta}\right) \tag{6}$$

where T is temperature (see e.g. Karoly & Hoskins, 1982).

When calculating the anomalous oceanic heating power due to advection, it is useful to look at the contribution from the zonally-averaged mean flow, $\mathbf{v} = (v, w)$, and its separation into contributions from changes in the mean flow, $\mathbf{v}$, and changes in the temperature gradient, ∇T, as follows:

$$\Delta\mathrm{P} = \iiint_V c_p\rho\Delta\dot{\mathrm{T}}\,dV' = -\iiint_V c_p\rho\Delta(\mathbf{v}.\boldsymbol{\nabla}\mathrm{T})\,dV' \approx -\iiint_V c_p\rho\left((\Delta\mathbf{v}).\boldsymbol{\nabla}\mathrm{T} + \mathbf{v}.\boldsymbol{\nabla}(\Delta\mathrm{T})\right)dV' \tag{7}$$

where c_p is the heat capacity of water at constant pressure, ρ is the density of (ocean) water, and V is the volume of water integrated over, and we have neglected higher order terms.

Oceanic currents are separated into Ekman and geostrophic components, driven by surface wind stress and pressure-gradient forces respectively. For the vertical velocity, utilising Sverdrup vorticity balance, these two components can be expressed as follows:

$$\mathrm{w_E}(\mathrm{z}=0) = -\frac{1}{\rho}\left(\frac{\partial\left(\frac{\tau_y}{f}\right)}{\partial x} - \frac{\partial\left(\frac{\tau_x}{f}\right)}{\partial y}\right) = -\mathrm{w_G}(\mathrm{z}=0) \quad (8)$$

$$\mathrm{w}_G(\mathrm{z}=-\mathrm{h}) = \mathrm{w_G}(\mathrm{z}=0) + \int_{-h}^{0}\frac{\beta v_G}{f}dz = \mathrm{w_G}(\mathrm{z}=0) + \int_{-h}^{0}\frac{\beta}{\rho f^2}\frac{\partial p}{\partial x}dz \quad (9)$$

where $\mathrm{w_E}$ and w_G are the Ekman and geostrophic vertical velocities, h is the depth below the ocean surface (z=0), τ_x and τ_y are the zonal and meridional components of surface wind stress respectively, and β is the Rossby parameter (Peixoto & Oort 1982).

3 Results

3.1 A model

Figure 1: Control values (contours) and anomalies (red/blue shading) in ensemble- and zonally-averaged zonal wind (a, c) and mass streamfunction (b, d), for experiment P01 (a, b) and T01 (c, d), averaged over years 0-30 and both hemispheres (i.e. $u_{30^0} = \left(u_{30^0\mathrm{N}} + u_{30^0\mathrm{S}}\right)/2$, $\psi_{30^0} = \left(\psi_{30^0\mathrm{N}} - \psi_{30^0\mathrm{S}}\right)/2$), in A model. Stippling indicates regions where the confidence levels in the experiment vs control values are above 95%, as measured by a two-tail student's t-test.

Figure 1 displays the equilibrium control values and anomalies in ensemble- and zonally-averaged zonal wind and mass streamfunction, in response to experiments P01 and T01, in the A model. In P01/T01, we observe a strengthening/weakening of the underlying atmospheric dynamics equatorward of about 50º, and a weakening/strengthening poleward. The Hadley cells, Ferrel cells, and midlatitude jet all strengthen/weaken, whilst the poleward flanks of the latter two get weaker/stronger, suggestive of an equatorward contraction/poleward expansion. Experiment P01 exhibits an overall stronger response, with peak changes in Ferrel cell/midlatitude jet strength of around -5Sv/+2m/s, vs. +2Sv/-1m/s for T01 (1Sv=10^9kg/s). The results of experiment U01in the A model are shown in figure S4, and resembled a weakened version of P01. This experiment shall thus be mostly omitted from subsequent subsections.

These results are in good agreement with those of previous studies using similar applied STPs, such as Haigh et al. (2005), Simpson et al. (2009), and White et al. (2020). Moreover, those of T01 bear a striking qualitative resemblance to studies simulating the

response of the Southern Hemisphere atmosphere to historical ozone depletion, such as Polvani et al. (2011), and Son et al. (2018).

Although not the main focus of this paper, experiments examining the transient and equilibrated response of the A model to the applied STPs revealed the mechanism responsible for this downwards transmission to be eddy-mean flow feedbacks, mediated by changes in the QG PV gradient originating around the tropopause (see chapter 3 of Trencham 2022), in agreement with Simpson et al. (2009), and White et al. (2020). This mechanism involves only synoptic-scale dynamics, and so can be simulated by even relatively coarse-resolution GCMs, with highly-parameterised physics, which explains why the atmospheric response appears to be generic across a wide range of GCMs and stratospheric forcings.

3.2 AO model

3.2.1 SST changes

Figure 2: Changes in ensemble- and zonally-averaged SSTs in experiment (a) P01 and (b) T01 in AO model, averaged over years 0-30 (red), 100-130 (green) and 200-230 (blue). Errorbars are calculated as the standard deviations of ensemble-mean values, calculated over the time dimension.

Figure 2 displays the changes in SST, seen in response to experiments P01 and T01 in the AO model, averaged over years 0-30, 100-130, and 200-230 of the spinup. In both experiments, a signal in the extratropics becomes evident relatively quickly, within the first 30 years, with experiment P01/T01 displaying a decrease/increase in SST south of 60ºS, and similarly north of 70ºN in P01. This is like the "slow" response, documented in Ferreira et al. (2015) and Seviour et al. (2016), to ozone depletion. In P01, we see also an increase in SST 45º-70ºN, and 40º-60ºS, in this timeperiod. Subsequently (years 100/200+), we also see significant increases/decreases in SST equatorward of about 60º in both hemispheres, whilst the polar cold/warm anomalies hold steady. These changes in low-latitude SST are larger (+0.5ºC vs. -0.2ºC) and faster (years 100+ vs. years 200+) in P01, corresponding to the larger magnitude atmospheric response (figure 1a,b). We note, from the significant changes in low-latitude SST between years 100-130 and 200-230, that the model has evidently not fully equilibrated, which can take up to 2000 years (see table 1). However, the general trend of SST changes appears clear by year 200+, with the relatively rapid high-latitude SST changes appearing steady, and low-latitude SSTs continuing to rise/fall gradually.

3.2.2 Changes in atmospheric response

Figure 3: As figure 1, but with the red/blue shading indicating the difference in anomalies between years 100-130 of P01 (a,b), and years 200-230 of T01 (c,d) in the AO model, vs. years 0-30 of P01/T01 in the A model. Stippling indicates regions where the confidence levels in the AO vs A model anomalies are above 95%, as measured by a two-tail student's t-test.

Figure 3 shows the differences (red/blue shading) in the response of the zonal winds and mass streamfunctions to experiment P01 and T01 in the AO model, compared to those seen in the A model (figure 1). So, areas of red/blue shading and stippling indicate regions where the atmospheric response in the AO model is significantly different to that seen in the A model.

We observe a poleward-/equatorward-shift in the midlatitude jet and Ferrel cell in experiments P01/T01, and a slight strengthening and poleward-expansion of the Hadley cell in P01. When superimposed on the underlying A model response (figure 1), this amounts to a slight strengthening and poleward-expansion of the signal in the tropics, and a slight weakening and poleward-shift of the signal in the extratropics. These changes in atmospheric response are evident from around year 100/200+ for experiment P01/T01, but not earlier (see figures S5-6).

3.3 AS model

The results of experiments P01 & T01 in the AS model were also examined and compared to those in the A model (see figures S7-8). For P01, a slight weakening of the Hadley cell, equatorial easterlies, and subtropical jet were observed, in contrast to the response seen in the AO model. For T01, there was a small equatorward shift of the midlatitude jet, similar to that seen in the AO model (figure 3c). In both cases, the SST changes were very different to that seen in the AO model, with local SST increases in regions of positive zonal wind anomalies in the extratropics (compare with figure 1a,c), and very small (max. 0.2ºC) tropical SST increases (figure S8).

This all serves to suggest that changes in the ocean heat transport - parameterised as fixed fluxes in the AS model – are crucial to providing the full SST anomaly, and feedback upon the atmosphere. We will therefore exclude the AS model from further analysis, and concentrate upon explaining the SST anomalies and atmospheric feedback we see in the AO model in the next subsection.

3.4 Mechanisms

3.4.1 Changes in atmospheric response

Figure 4: Zonally-averaged SST anomalies corresponding to: full SST anomaly in P01 in AO model, averaged over years 0-300 (black curve), its extratropical component only, minus a uniform +0.3K SST increase (blue curve), a uniform +0.3K SST increase (red curve), and the full SST anomaly in U01 in the AS model, averaged over years 25-50 (green curve).

As outlined in section 3.2.2, significant modifications to the atmospheric responses of the A model, detailed in section 3.1, were only seen after 100/200+ years for P01/T01 in the AO model. Since the only differences between the A and AO models are the absence/presence of a fully dynamical ocean with variable SST, it stands to reason that these changes must be caused by the SST changes shown in figure 2. This is confirmed by looking at the atmospheric response in the A model to the applied SST perturbation

only (figures 5, S10, a-b), which qualitatively resembles the full anomaly (figure 3), although further, non-linear feedbacks may be required to obtain the full atmospheric response.

Further, since the only SST changes seen over this timeperiod (years 30-100/200) are near-uniform increases/decreases in SST in the low-to-mid latitudes, it is these SST changes which we expect to be responsible for driving the difference in atmospheric response. This is confirmed by looking at the atmospheric response in the A model to a range of SST perturbations, representing different aspects of the full AO SST anomalies (figures 5, S10, a-b): uniform +/-0.3ºC SST perturbations (figures 5, S10,e-f) produce an atmospheric response qualitatively similar to that caused by the full SST perturbation, whilst application only of the changes in extratropical meridional gradient produce an opposite/negligible atmospheric response (figures 5, S10,c-d). However, the atmospheric response to the full SST perturbations does not appear fully linearly separable into these two responses (figures 5, S10,g-h), probably due to non-linear atmospheric feedbacks. Still, these results lend at least some support to the hypothesis that the changes in low-to-midlatitude SST are responsible for triggering the observed atmospheric changes seen in the AO model vs the A model.

Figure 5: As figure 1, but with red/blue shading indicating the anomalous response to the applied SST anomalies of figure 4: the full SST anomaly (a,b), the extratropical SST anomaly (c,d), the uniform +0.3K anomaly (e,f), and the linear combination of (c,d) + (e,f) (g,h).

Figure 6: Atmospheric response to near-uniform SST increase (figure 4, green curve), averaged over days 1-5 of spinup: anomalous mass streamfunction (contours, Sv) and zonal wind (red/blue shading, m/s) (a); anomalous residual streamfunction (contours, Sv) and residual Coriolis torque, $f\tilde{v}$ (red/blue shading, m/s/day) (b); anomalous meridional PV gradient, q_{φ} (contours, /day), mass-weighted EP fluxes (arrows) and EP flux divergence (red/blue shading, /day) (c); anomalous 3rd meridional PV gradient component in equation (6) (contours, /day) and temperature (shading, K) (d).

To investigate how the atmospheric response to these SST changes was initiated, we look at the initial atmospheric response to a near-uniform SST perturbation (green curve of figure 4), as outlined in section 2. The response to this SST anomaly was analysed because of its qualitative resemblance to that due to the full P01 SST anomaly in the AO model, but stronger magnitude (compare figures S11 & 5a,b). The atmospheric response during the first 5 days of forcing is shown in figure 6. We observe a greatly strengthened Hadley cell, and a more baroclinic subtropical jet, with positive/negative zonal wind anomalies in the upper/lower troposphere (figure 6a), the former powering the latter through Coriolis acceleration (figure 6b, red/blue shading). The Hadley cell itself is likely powered by the strong tropical heating (figure 6d, shading), resulting from tropical convection, enhancing the equator-to-pole temperature gradient (e.g. Vallis 2006). The enhanced subtropical baroclinicity creates an anomalous dipole in the meridional PV gradient in the upper subtropical troposphere (figure 6c, contours) - driven primarily by the third component of equation (6) (figure 6d, contours) - which acts as a waveguide to the anomalous EP fluxes generated in the subtropics-to-midlatitudes (figure 6c, arrows).

The net effect of this dipole, combined with eddy-mean flow feedbacks, will be to cause zonal momentum to be carried away from the subtropical upper troposphere, and towards the midlatitude lower troposphere, accelerating the eddy-driven midlatitude jet and circulation. For further details, see chapter 6 of Trencham (2022). This mechanism is similar to that detailed in Hou (1998), and agrees with previous studies looking at the effect of tropical diabatic heating on the Hadley circulation itself (Held & Hou 1980; Frierson et al. 2007), and its downstream dynamical impacts (Kang & Polvani 2011; Ceppi & Hartmann 2013; Mbengue & Schneider 2018).

A near-uniform SST increase/decrease, therefore, acts to strengthen/weaken the underlying mean zonal winds and circulations, through its effect upon the tropical temperatures and circulation, creating a region of enhanced/diminished subtropical baroclinicity, with downstream impacts upon the eddy-driven midlatitude jet and circulation.

In many ways, the mechanism controlling the atmospheric response to SST perturbations is similar to that controlling the response to STPs. Both involve modifications to the strength and position of the midlatitude jet and circulation, mediated by synoptic-scale eddies via changes in baroclinicity/QG PV gradient. A fundamental difference, though, is how applied SST perturbations directly modify – via changes in the absolute temperature and meridional temperature gradient - the available energy for eddy generation, and the atmospheric baroclinicity.

3.4.2 Changes in ocean heat content (OHC)

Figure 7 shows the time-evolution of anomalous ocean heating terms, integrated over the top 1800m, and over the low-/high-latitudes, for experiment P01 in the AO model (see figure S12 for the corresponding figure for T01). We see how, after the first ~20years, heating in the tropics is powered primarily by advective heating anomalies (figure 7a, green curve), which in turn is driven by anomalous downwelling for the first ~50years (figure 7b, green curve), and a combination of that and passive advection by the meridional currents subsequently (figure 7b, magenta curve). In the Southern Ocean region, anomalous cooling occurs in the first ~50years (figure 7c, black curve), and is clearly driven by anomalous downwelling (figure 7d, green curve). The Northern high-latitudes tells a similar story to the Southern Ocean (figures 7e-f), although, similar to the tropics, cooling by passive meridional advection is of a similar magnitude to that by anomalous downwelling currents (figure 7f, magenta & green curves). However, heating by anomalous poleward advection (figure 7f, yellow curve) overrides this to give a net heating by meridional advection (figure 7f, red curve). It is noteworthy that the heating/cooling due to anomalous vertical and meridional currents is always in opposition to each other (figures 7b,d,f, green & yellow curves), as in the mechanism of Ferreira et al. (2015).

Figure 8 shows the changes in ocean temperature, meridional, and vertical currents for P01 in the AO model (see figure S13 for the corresponding figure for T01). We see very deep temperature increases in the low-latitudes, 40S-40N, extending down to around 1600m at 30S (figure 6a). These are centered around 30S/N and 500/1000m respectively,

which appears to correspond approximately to the bottom, poleward, downwelling branches of a tropical Ekman cell (see figures 6b,c). This subtropical downwelling is clearly strengthened, as is the midlatitude upwelling, whilst anomalous downwelling occurs around the poles (figure 6c). Most of these changes in vertical currents is geostrophically-driven (figure 6d), the bulk of which is due to changes in the Ekman pumping, as indicated by the relative vertical-uniformity of the geostrophic anomalies.

Figure 7: The anomalous oceanic heating rates in P01 in AO model, integrated over 0-1800m, and 39S-39N (a,b), 89S-39S (c,d) and 39N-89N (e,f). In the left panel (a,c,e): black=net heating, black stippled = surface flux + advective + diffusive heating, red = surface flux heating, blue = advective + diffusive heating, magenta = diffusive heating, green = advective heating, cyan = mean-flow advective heating. In the right panel (b,d,f): black = total mean-flow advective heating, blue/red = total vertical/meridional mean-flow heating, green/yellow = heating due to anomalous vertical/meridional currents (1^{st} term on RHS of equation (7)), cyan/magenta = heating due to anomalous vertical/meridional temperature gradients (2^{nd} term on RHS of equation (7)).

Figure 8. Control values (contours) and anomalies (red/blue shading) of zonal-mean oceanic: temperature, (K, a), meridional velocity (mm/s, b; positive = northward), vertical velocity (m/day, c; positive = upward), and geostrophic vertical velocity (m/day, d; positive = upward; see equation (9)), with (a) averaged over years 250-300, and (b-d) averaged over years 0-300. Stippling indicates regions where the confidence levels in the anomalies are above 95%, as measured by a two-tail student's t-test.

Therefore, what appears to be happening in experiment P01 in the AO model is as follows: anomalous Ekman downwelling in the subtropics/poles drives local, deep increases/decreases in ocean temperature (opposite sign due to polar temperature inversion), throughout the thermocline. Slow, passive meridional advection and diffusion then redistributes this throughout the rest of the tropical thermocline, appearing at the surface after 100s of years. The converse explanation holds for T01 (see figures S12-13), although the magnitudes and timescales of oceanic changes is generally half and double those in P01 respectively, likely due to the weaker atmospheric response seen in T01 vs. P01 (see figure 1c,d). Also, the low-latitude surface heat fluxes have a positive heat flux into the ocean for the first ~200 years (see figure S12a, red curves), explaining the initial positive low-latitude SST anomaly seen in T01 (figure 2b, red & green curves).

As far as interhemispheric-asymmetry in the extratropics is concerned, we note a weaker vertical temperature gradient in the northern vs. southern polar region (figure 8a). This would cause the same magnitude of induced downwelling/upwelling to have a weaker cooling/heating, which is indeed what we see (see figure 2). This weaker polar cooling/warming may also allow for the warming/cooling effects of anomalous poleward/equatorward surface Ekman currents to be more prominent, causing the warm/cold anomaly we observe around 60N in P01/T01. Alternatively, or additionally, this could be caused by the local vertical temperature inversion we see there (see figure 8a) – probably caused by the poleward overturning circulation we see in the top 1200m of the extratropical NH (figure 8c), transporting warm tropical water poleward beneath

the Ekman layer - superimposed on an anomalous upwelling/downwelling (figures 8c, S13c), causing local warming/cooling.

3.4.3 Overall mechanism

The emergent picture of oceanic feedbacks upon STPs in the AO model is as follows. Applied positive STPs cause an equatorward/poleward (P01/T01) shift in the tropospheric midlatitude circulation and jet. This causes an equatorward/poleward shift in the zero surface wind stress line, causing an anomalous Ekman transport of heat towards/away from the tropics, and gradual rise/fall in tropical SST, on a diffusive timescale. Through its enhancing/diminishing effect upon tropical temperatures and equator-to-pole temperature gradients, this drives a strengthened/weakened and poleward-expanded/equatorward-contracted Hadley cell and subtropical jet, in turn generating stronger/weaker poleward eddy heat and momentum fluxes, driving a strengthened/weakened and poleward-/equatorward-shifted midlatitude jet and circulation. The net result is an amplification/reduction of the underlying atmospheric zonal-mean jets and circulation, causing a positive feedback (strengthening) upon the STP signal in the tropics, and a negative feedback (weakening) upon the STP signal in the extratropics.

4 Discussion and Conclusions

We have tested the hypothesis that atmosphere-ocean coupling affects the atmospheric response to positive STPs by imposing such STPs in three different versions of the MITgcm, with varying degrees of atmosphere-ocean coupling present.

From section 3.2.2, it is evident that atmosphere-ocean coupling is significant, causing a general strengthening/weakening and poleward-expansion/-shift to the underlying atmospheric response in the tropics/extratropics, after 100/200+ years in the AO model. In other words, the response to positive STPs in the tropics experiences a positive feedback, and that in the extratropics a negative feedback. The lack of significance prior to this, and the inability of the AS model to capture the full atmospheric and SST changes, suggested a key role played by changes in the ocean dynamics, and would explain the apparent lack of impact seen in previous, shorter-term studies (Sigmond et al. 2010; Seviour et al. 2017; Son et al. 2018). Indeed, section 3.4.2 found the changes in tropical SST to be driven primarily by changes in the Ekman transport, itself attributable to the changes in surface wind stress. Such tropical SST changes were found, in section 3.4.1, to be primarily responsible for the observed atmospheric changes, via their impact upon the tropical Hadley circulation and subtropical jet, and downstream impacts upon the eddy heat and momentum transport. We note that, whilst longer (100+ years) simulations are necessary to identify this response, an ensemble of runs may not be, owing to model sensitivity to tropical SST changes.

Broadly speaking, the tropical SST changes allow the Hadley cell to further strengthen/weaken, and to expand/contract latitudinally. This drives a corresponding strengthening/weakening and poleward-/equatorward-shift in the midlatitude jets and circulation, displacing the underlying extratropical atmospheric changes towards the poles. Applied to Earth, the implication is that the Southern Hemisphere midlatitude jet and circulation – whose poleward-shift since the 1970s has

been observed, and attributed to declining levels of stratospheric ozone (e.g. Polvani et al. 2011) - may, in the coming 100+ years, shift further poleward. This is particularly likely if levels of greenhouse gases continue to rise throughout the 21st century, cancelling or overriding the effects of stratospheric ozone recovery (Gerber & Son 2014).

In this paper, our focus has been on testing the effect of oceanic feedbacks on the tropospheric response to positive STPs, using a relatively simple model, setup, and applied STPs. It would be instructive to see whether similar results arise from use of a more complex, realistic model and setup, with STPs that more closely resemble those seen due to e.g. stratospheric ozone depletion. In particular, sea ice, which was excluded from this model, may impact the polar SST changes significantly. This would also allow for greater quantitative clarification of the precise atmospheric/oceanic changes and timescales involved. Further, it may be worth repeating similar experiments using a higher-resolution AO model, capable of resolving mesoscale ($\lesssim$100km) ocean eddies. It has been noted (e.g. Czaja et al. 2019) that such increased model resolution can lead to an enhanced representation of extratropical atmosphere-ocean coupled processes, such as cyclogenesis. This may significantly modify the atmospheric response to STPs by the extratropical SST anomalies, and at shorter timescales than that caused by tropical SST anomalies, owing to the former's relatively fast (~30 years) appearance in model simulations.

Lastly, a useful extension of the work in this paper would be to apply a similar analysis to the uncoupled/coupled atmospheric response to increased levels of greenhouse gases, possibly combined with stratospheric ozone changes. Whilst the changes in atmospheric dynamics would be similar those seen in experiment T01, increases in tropospheric temperature may drive significantly different SST anomalies, especially in the low-to-midlatitudes, which cooled under T01 in the AO model. This may significantly impact our assessment of if and how oceanic feedbacks need to be accounted for when analysing the long-term tropospheric response.

Acknowledgments

We extend our thanks to the editors for their time and effort in reviewing and providing comment on this paper. We acknowledge the work of John Marshall and others in developing, updating, and providing supporting documentation for the MITgcm. Special thanks to Matthew Kasoar for his help with running and troubleshooting the MITgcm, and to Minyi Liang, and Peter Shatwell. This work was funded by the UK Natural Environment Research Council through sponsorship of NT on the Science and Solutions for a Changing Planet Doctoral Training Partnership.

Open Research

The MIT General Circulation Model, used to conduct the simulations presented in sections 2 and 3, is available at https://doi.org/10.5281/zenodo.1409237, and developed openly at https://mitgcm.org/(Campin et al. 2023).

References

Andrews, D. G., & Mcintyre, M. E. (1976). Planetary waves in horizontal and vertical shear: The generalized Eliassen-Palm relation and the mean zonal acceleration. Journal of Atmospheric

514 Sciences, 33(11), 2031-2048. https://doi.org/10.1175/1520-
515 0469(1976)033<2031:PWIHAV>2.0.CO;2
516 Andrews, M. B., Knight, J. R., & Gray, L. J. (2015). A simulated lagged response of the North
517 Atlantic Oscillation to the solar cycle over the period 1960–2009. Environmental Research
518 Letters, 10(5), 054022. https://doi.org/10.1088/1748-9326/10/5/054022
519 Baldwin, M. P., & Dunkerton, T. J. (1999). Propagation of the Arctic Oscillation from the
520 stratosphere to the troposphere. *Journal of Geophysical Research: Atmospheres*, *104*(D24),
521 30937-30946. https://doi.org/10.1029/1999JD900445
522 Cai, W. (2006). Antarctic ozone depletion causes an intensification of the Southern Ocean super-
523 gyre circulation. In Geophysical Research Letters (Vol. 33, Issue 3). American Geophysical
524 Union (AGU). https://doi.org/10.1029/2005gl024911
525 Cai, W., & Cowan, T. (2007). Trends in Southern Hemisphere Circulation in IPCC AR4 Models
526 over 1950–99: Ozone Depletion versus Greenhouse Forcing. In Journal of Climate (Vol. 20,
527 Issue 4, pp. 681–693). American Meteorological Society. https://doi.org/10.1175/jcli4028.1
528 Jean-Michel Campin; Patrick Heimbach; Martin Losch; Gael Forget; edhill3; Alistair Adcroft;
529 amolod; Dimitris Menemenlis; dfer22; Oliver Jahn; Chris Hill; Jeff Scott; stephdut; Matt
530 Mazloff; Baylor Fox-Kemper; antnguyen13; Ed Doddridge; Ian Fenty; Michael Bates; Timothy
531 Smith; AndrewEichmann-NOAA; mitllheisey; Jonathan Lauderdale; Torge Martin; Ryan
532 Abernathey; Ou Wang; samarkhatiwala; dngoldberg; hongandyan; Bruno Deremble. (2023).
533 MITgcm/MITgcm: ckeckpoint68: August 2, 2023 Release [Software]. Zenodo.
534 https://doi.org/10.5281/zenodo.1409237 .

Ceppi, P., & Hartmann, D. L. (2013). On the Speed of the Eddy-Driven Jet and the Width of the Hadley Cell in the Southern Hemisphere. In Journal of Climate (Vol. 26, Issue 10, pp. 3450–3465). American Meteorological Society. https://doi.org/10.1175/jcli-d-12-00414.1

Czaja, A., Frankignoul, C., Minobe, S., & Vannière, B. (2019). Simulating the Midlatitude Atmospheric Circulation: What Might We Gain From High-Resolution Modeling of Air-Sea Interactions? In Current Climate Change Reports (Vol. 5, Issue 4, pp. 390–406). Springer Science and Business Media LLC. https://doi.org/10.1007/S50641-019-00148-5

Edmon Jr, H. J., Hoskins, B. J., & McIntyre, M. E. (1980). Eliassen-Palm cross sections for the troposphere. Journal of Atmospheric Sciences, 37(12), 2600-2616. https://doi.org/10.1175/1520-0469(1980)037<2600:EPCSFT>2.0.CO;2

Ferreira, D., Marshall, J., Bitz, C. M., Solomon, S., & Plumb, A. (2015). Antarctic Ocean and Sea Ice Response to Ozone Depletion: A Two-Time-Scale Problem. In Journal of Climate (Vol. 28, Issue 3, pp. 1206–1226). American Meteorological Society. https://doi.org/10.1175/jcli-d-14-00313.1

Frierson, D. M. W., Lu, J., & Chen, G. (2007). Width of the Hadley cell in simple and comprehensive general circulation models. In Geophysical Research Letters (Vol. 34, Issue 18). American Geophysical Union (AGU). https://doi.org/10.1029/2007gl031115

Geen, R., Czaja, A., & Haigh, J. D. (2016). The effects of increasing humidity on heat transport by extratropical waves. In Geophysical Research Letters (Vol. 43, Issue 15, pp. 8314–8321). American Geophysical Union (AGU). https://doi.org/10.1002/2016gl070214

Gerber, E. P., & Son, S.-W. (2014). Quantifying the Summertime Response of the Austral Jet Stream and Hadley Cell to Stratospheric Ozone and Greenhouse Gases. In Journal of Climate

(Vol. 27, Issue 14, pp. 5538–5559). American Meteorological Society. https://doi.org/10.1175/jcli-d-13-00539.1

Haigh, J. D., Blackburn, M., & Day, R. (2005). The response of tropospheric circulation to perturbations in lower-stratospheric temperature. Journal of Climate, 18(17), 3672-3685. https://doi.org/10.1175/JCLI3472.1

Held, I. M., & Hou, A. Y. (1980). Nonlinear axially symmetric circulations in a nearly inviscid atmosphere. Journal of the Atmospheric Sciences, 37(3), 515-533.

Hou, A. Y. (1998). Hadley Circulation as a Modulator of the Extratropical Climate. In Journal of the Atmospheric Sciences (Vol. 55, Issue 14, pp. 2437–2457). American Meteorological Society. https://doi.org/10.1175/1520-0469(1998)055<2437:hcaamo>2.0.co;2

Kang, S. M., & Polvani, L. M. (2011). The Interannual Relationship between the Latitude of the Eddy-Driven Jet and the Edge of the Hadley Cell. In Journal of Climate (Vol. 24, Issue 2, pp. 563–568). American Meteorological Society. https://doi.org/10.1175/2010jcli4077.1

Karoly, D. J., & Hoskins, B. J. (1982). Three dimensional propagation of planetary waves. Journal of the Meteorological Society of Japan. Ser. II, 60(1), 109-123. https://doi.org/10.2151/jmsj1965.60.1_109

Karpechko, A. Y. E., Maycock, A. C., Abalos, M., Akiyoshi, H., Arblaster, J. M., Garfinkel, C. I., ... & Sigmond, M. (2019). Stratospheric ozone changes and climate. In *Scientific Assessment of Ozone Depletion: 2018*. World Meteorological Organization.

Klinger, B. A., & Marotzke, J. (2000). Meridional Heat Transport by the Subtropical Cell. In Journal of Physical Oceanography (Vol. 30, Issue 4, pp. 696–705). American Meteorological Society. https://doi.org/10.1175/1520-0485(2000)030<0696:mhtbts>2.0.co;2

579 Kushner, P. J., & Polvani, L. M. (2004). Stratosphere–troposphere coupling in a relatively simple
580 AGCM: The role of eddies. *Journal of climate*, *17*(3), 629-639. https://doi.org/10.1175/1520-
581 0442(2004)017<0629:SCIARS>2.0.CO;2
582 Lorenz, D. J., & DeWeaver, E. T. (2007). Tropopause height and zonal wind response to global
583 warming in the IPCC scenario integrations. In Journal of Geophysical Research: Atmospheres
584 (Vol. 112, Issue D10). American Geophysical Union (AGU).
585 https://doi.org/10.1029/2006jd008087
586 Mbengue, C., & Schneider, T. (2018). Linking Hadley Circulation and Storm Tracks in a
587 Conceptual Model of the Atmospheric Energy Balance. In Journal of the Atmospheric Sciences
588 (Vol. 75, Issue 3, pp. 841–856). American Meteorological Society. https://doi.org/10.1175/jas-d-
589 17-0098.1
590 Menary, M. B., & Scaife, A. A. (2014). Naturally forced multidecadal variability of the Atlantic
591 meridional overturning circulation. Climate dynamics, 42, 1347-1362.
592 https://doi.org/10.1007/s00382-013-2028-x
593 O'Callaghan, A., Joshi, M., Stevens, D., & Mitchell, D. (2014). The effects of different sudden
594 stratospheric warming types on the ocean. Geophysical Research Letters, 41(21), 7739-7745.
595 https://doi.org/10.1002/2014GL062179
596 O'Gorman, P. A., & Schneider, T. (2008). The Hydrological Cycle over a Wide Range of
597 Climates Simulated with an Idealized GCM. In Journal of Climate (Vol. 21, Issue 15, pp. 3815–
598 3832). American Meteorological Society. https://doi.org/10.1175/2007jcli2065.1
599 Omrani, N. E., Keenlyside, N. S., Bader, J., & Manzini, E. (2014). Stratosphere key for
600 wintertime atmospheric response to warm Atlantic decadal conditions. Climate Dynamics, 42,
601 649-663. https://doi.org/10.1007/s00382-013-1860-3

602 Peixoto, J. P., Oort, A. H., & Lorenz, E. N. (1992). Physics of climate (Vol. 520). New York:
603 American Institute of Physics.
604 Polvani, L. M., & Kushner, P. J. (2002). Tropospheric response to stratospheric perturbations in
605 a relatively simple general circulation model. *Geophysical Research Letters*, *29*(7), 18-1.
606 https://doi.org/10.1029/2001GL014284
607 Polvani, L. M., Waugh, D. W., Correa, G. J. P., & Son, S.-W. (2011). Stratospheric Ozone
608 Depletion: The Main Driver of Twentieth-Century Atmospheric Circulation Changes in the
609 Southern Hemisphere. In Journal of Climate (Vol. 24, Issue 3, pp. 795–812). American
610 Meteorological Society. https://doi.org/10.1175/2010jcli3772.1
611 Reichler, T., Kim, J., Manzini, E., & Kröger, J. (2012). A stratospheric connection to Atlantic
612 climate variability. Nature Geoscience, 5(11), 783-787. https://doi.org/10.1038/ngeo1586
613 Scaife, A. A., Ineson, S., Knight, J. R., Gray, L., Kodera, K., & Smith, D. M. (2013). A
614 mechanism for lagged North Atlantic climate response to solar variability. Geophysical Research
615 Letters, 40(2), 434-439. https://doi.org/10.1002/grl.50099
616 Seviour, W. J. M., Gnanadesikan, A., & Waugh, D. W. (2016). The Transient Response of the
617 Southern Ocean to Stratospheric Ozone Depletion. In Journal of Climate (Vol. 29, Issue 20, pp.
618 7383–7396). American Meteorological Society. https://doi.org/10.1175/jcli-d-16-0198.1
619 Seviour, W. J. M., Waugh, D. W., Polvani, L. M., Correa, G. J. P., & Garfinkel, C. I. (2017).
620 Robustness of the Simulated Tropospheric Response to Ozone Depletion. In Journal of Climate
621 (Vol. 30, Issue 7, pp. 2577–2585). American Meteorological Society.
622 https://doi.org/10.1175/jcli-d-16-0817.1

623 Sigmond, M., Fyfe, J. C., & Scinocca, J. F. (2010). Does the ocean impact the atmospheric
624 response to stratospheric ozone depletion? In Geophysical Research Letters (Vol. 37, Issue 12, p.
625 n/a-n/a). American Geophysical Union (AGU). https://doi.org/10.1029/2010gl043773
626 Simpson, I. R., Blackburn, M., & Haigh, J. D. (2009). The Role of Eddies in Driving the
627 Tropospheric Response to Stratospheric Heating Perturbations. In Journal of the Atmospheric
628 Sciences (Vol. 66, Issue 5, pp. 1347–1365). American Meteorological Society.
629 https://doi.org/10.1175/2008jas2758.1
630 Son, S.-W., Han, B.-R., Garfinkel, C. I., Kim, S.-Y., Park, R., Abraham, N. L., Akiyoshi, H.,
631 Archibald, A. T., Butchart, N., Chipperfield, M. P., Dameris, M., Deushi, M., Dhomse, S. S.,
632 Hardiman, S. C., Jöckel, P., Kinnison, D., Michou, M., Morgenstern, O., O'Connor, F. M., …
633 Zeng, G. (2018). Tropospheric jet response to Antarctic ozone depletion: An update with
634 Chemistry-Climate Model Initiative (CCMI) models. In Environmental Research Letters (Vol.
635 13, Issue 5, p. 054024). IOP Publishing. https://doi.org/10.1088/1748-9326/aabf21
636 Staten, P. W., & Reichler, T. (2013). On the ratio between shifts in the eddy-driven jet and the
637 Hadley cell edge. In Climate Dynamics (Vol. 42, Issues 5–6, pp. 1229–1242). Springer Science
638 and Business Media LLC. https://doi.org/10.1007/s00382-013-1905-7
639 Trencham, N. E. (2022). Stratosphere-Troposphere Coupling and Oceanic Feedbacks in an
640 Aquaplanet Model, PhD thesis. Imperial College London.
641 Vallis, G. K. (2006). Atmospheric and Oceanic Fluid Dynamics: Fundamentals and Large-scale
642 Circulation. Cambridge University Press.
643 Wang, G., Cai, W., & Purich, A. (2014). Trends in Southern Hemisphere wind-driven circulation
644 in CMIP5 models over the 21st century: Ozone recovery versus greenhouse forcing. In Journal

645 of Geophysical Research: Oceans (Vol. 119, Issue 5, pp. 2974–2986). American Geophysical
646 Union (AGU). https://doi.org/10.1002/2013jc009589
647 White, I. P., Garfinkel, C. I., Gerber, E. P., Jucker, M., Hitchcock, P., & Rao, J. (2020). The
648 Generic Nature of the Tropospheric Response to Sudden Stratospheric Warmings. In Journal of
649 Climate (Vol. 33, Issue 13, pp. 5589–5610). American Meteorological Society.
650 https://doi.org/10.1175/jcli-d-19-0697.1

Figure 1.

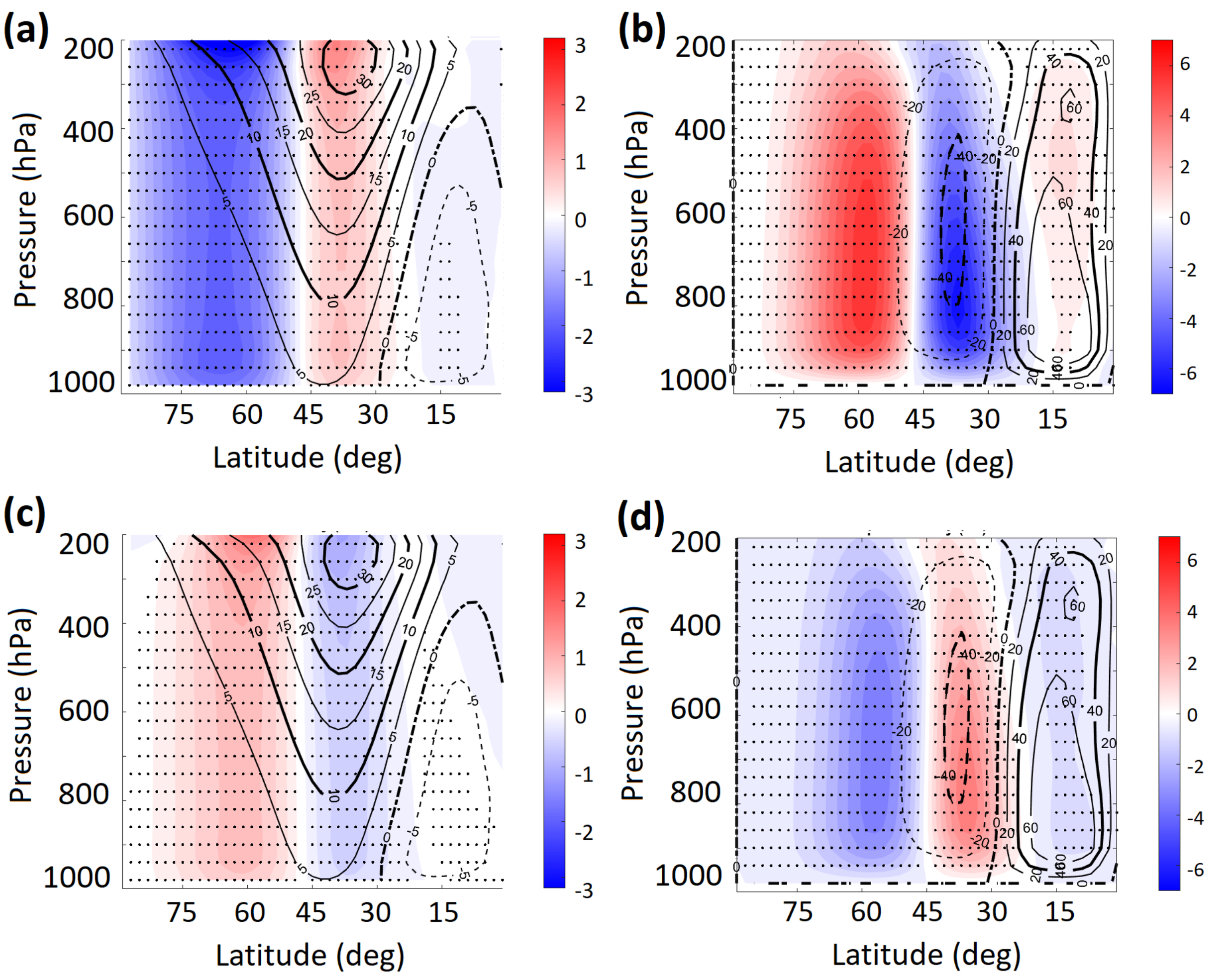
(a)
(b)
(c)
(d)
Pressure (hPa)
Latitude (deg)
200
400
600
800
1000
75
60
45
30
15
3
2
1
0
-1
-2
-3
6
4
2
0
-2
-4
-6

Figure 2.

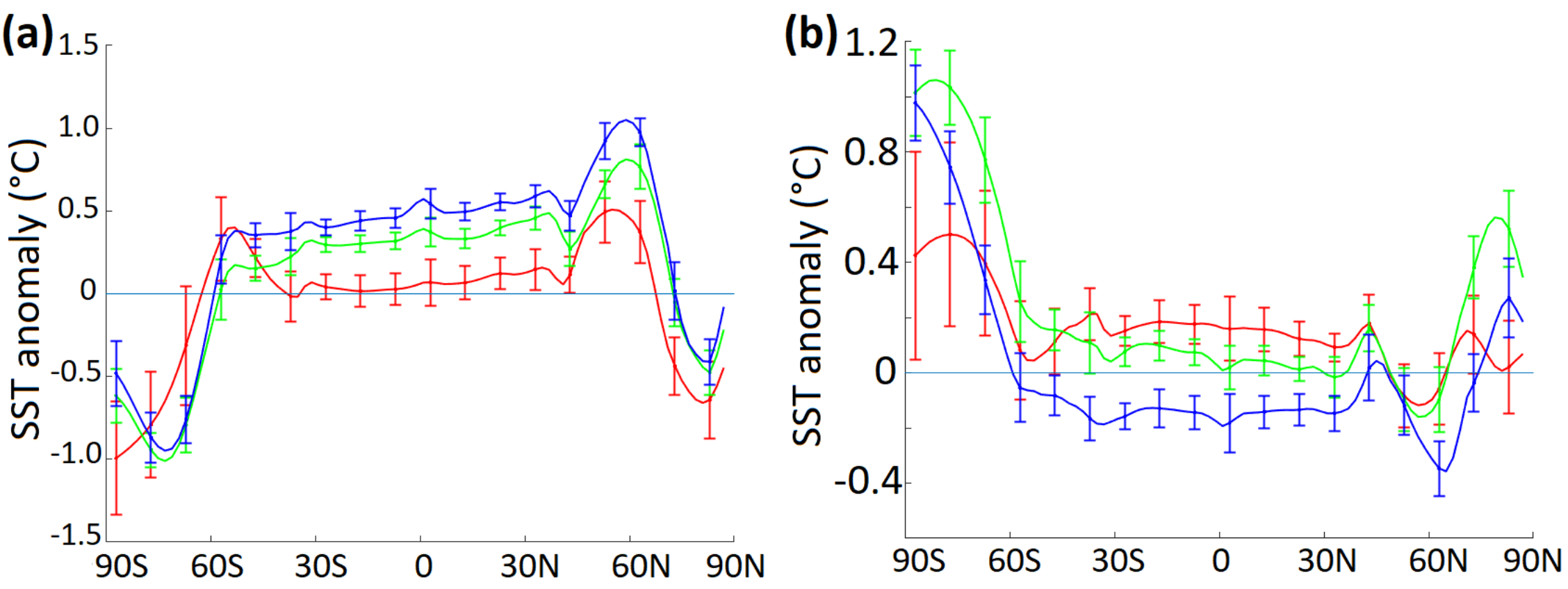
(a)
SST anomaly (°C)
1.5
1.0
0.5
0
-0.5
-1.0
-1.5
90S
60S
30S
0
30N
60N
90N
(b)
SST anomaly (°C)
1.2
0.8
0.4
0
-0.4
90S
60S
30S
0
30N
60N
90N

Figure 3.

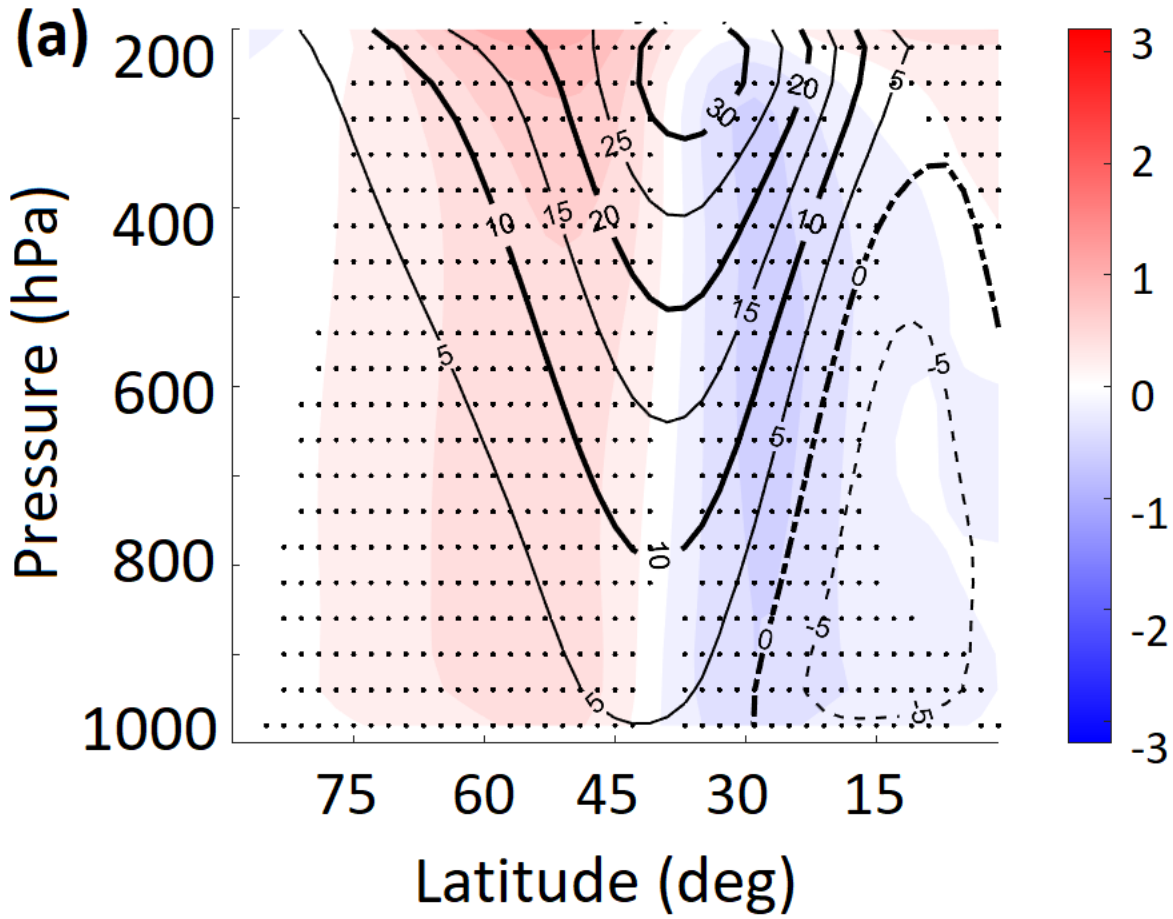
(a)
Pressure (hPa)
200
400
600
800
1000
75
60
45
30
15
Latitude (deg)
3
2
1
0
-1
-2
-3

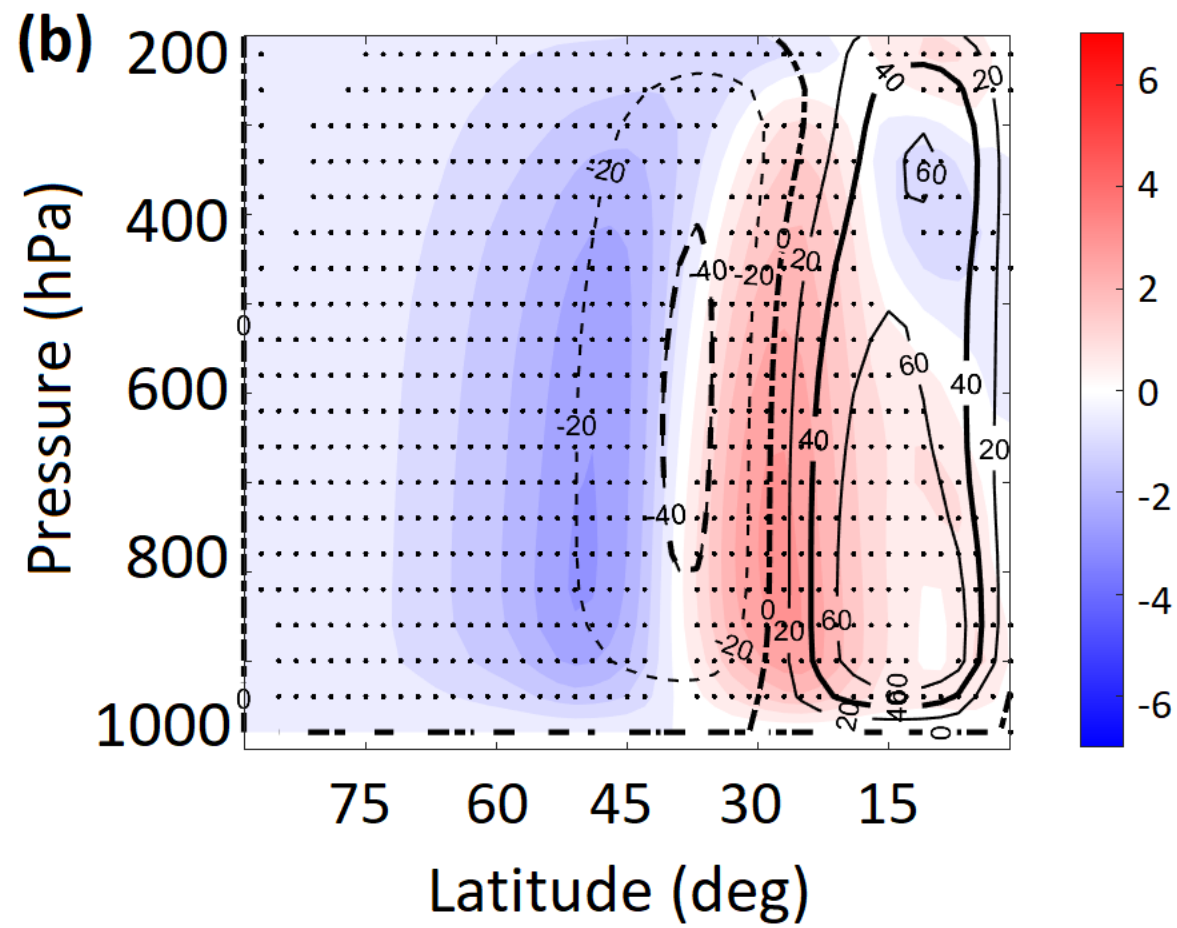
(b)
Pressure (hPa)
200
400
600
800
1000
75
60
45
30
15
Latitude (deg)
6
4
2
0
-2
-4
-6

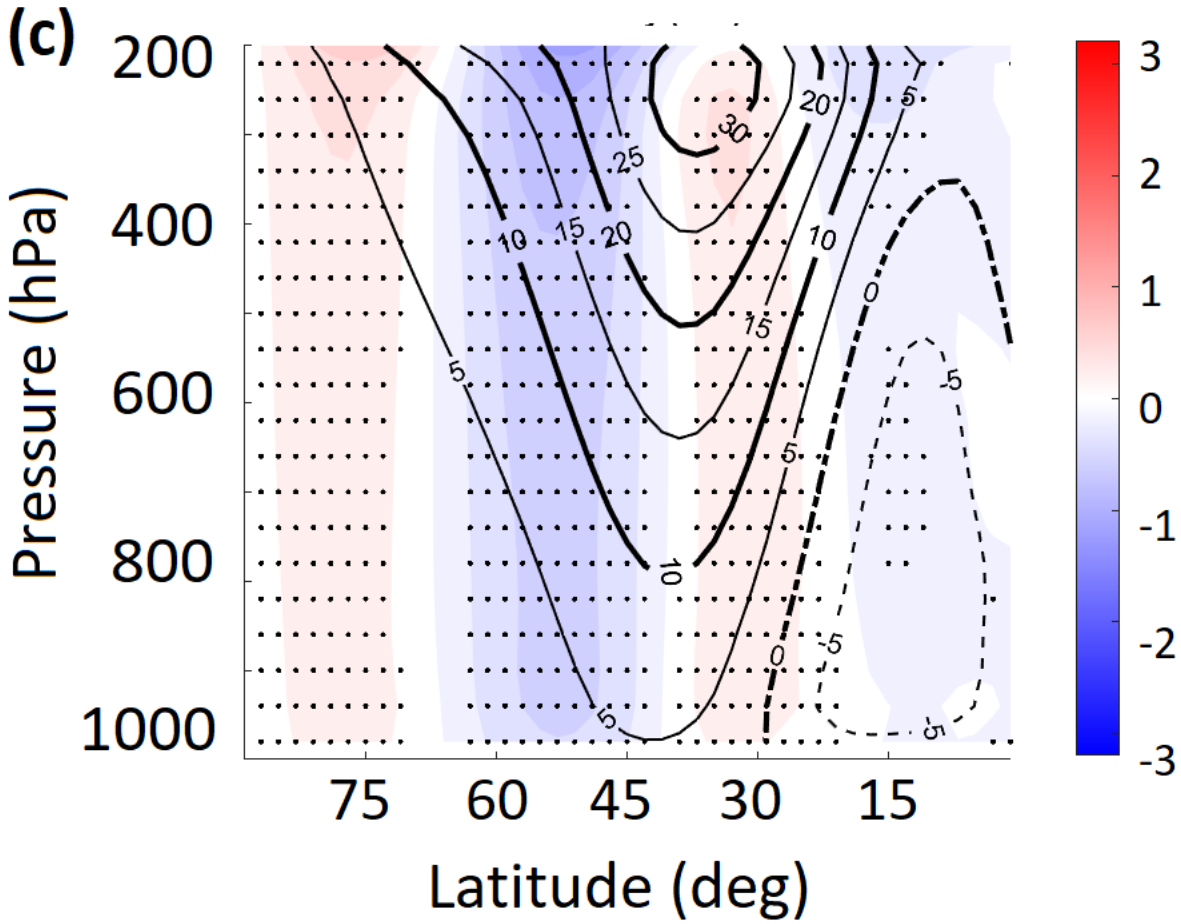
(c)
Pressure (hPa)
200
400
600
800
1000
75
60
45
30
15
Latitude (deg)
3
2
1
0
-1
-2
-3

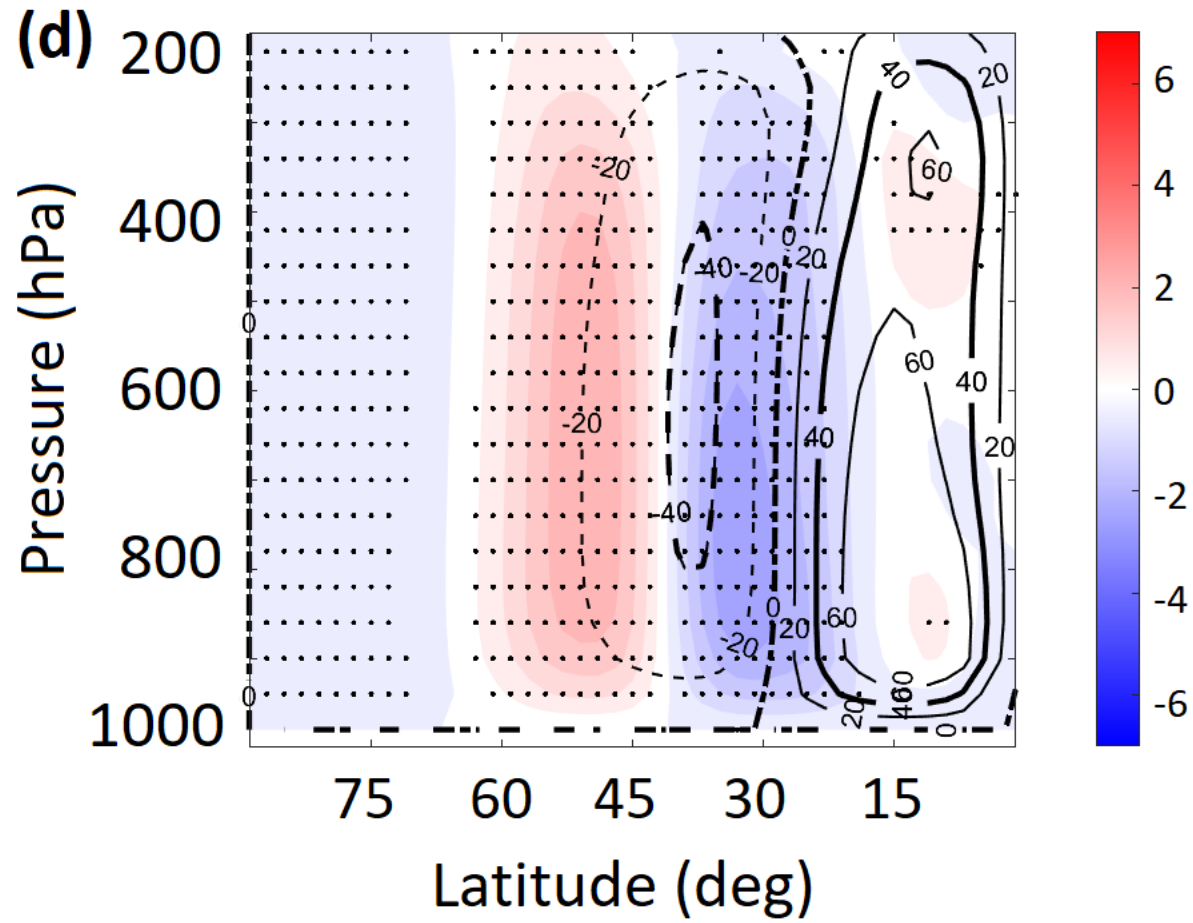
(d)
Pressure (hPa)
200
400
600
800
1000
75
60
45
30
15
Latitude (deg)
6
4
2
0
-2
-4
-6

Figure 4.

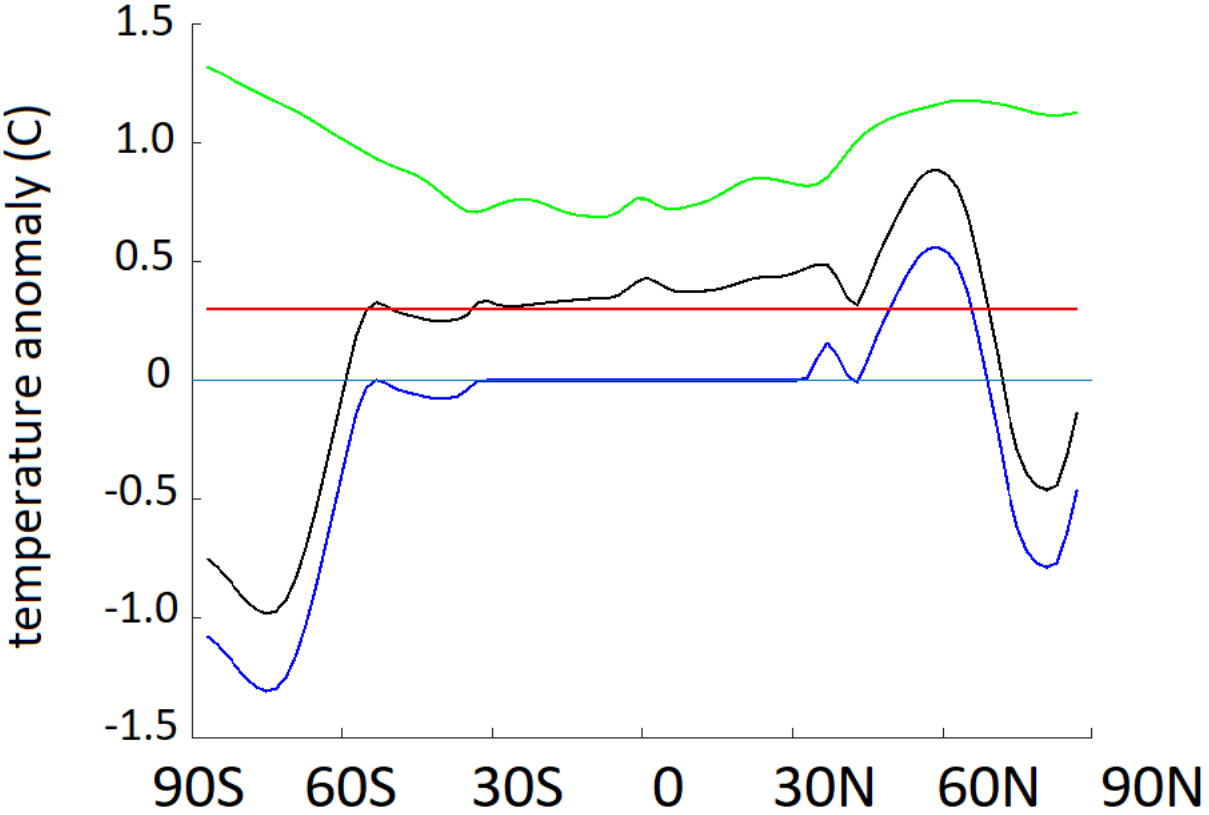
temperature anomaly (C)
1.5
1.0
0.5
0
-0.5
-1.0
-1.5
90S
60S
30S
0
30N
60N
90N

Figure 5.

(a)

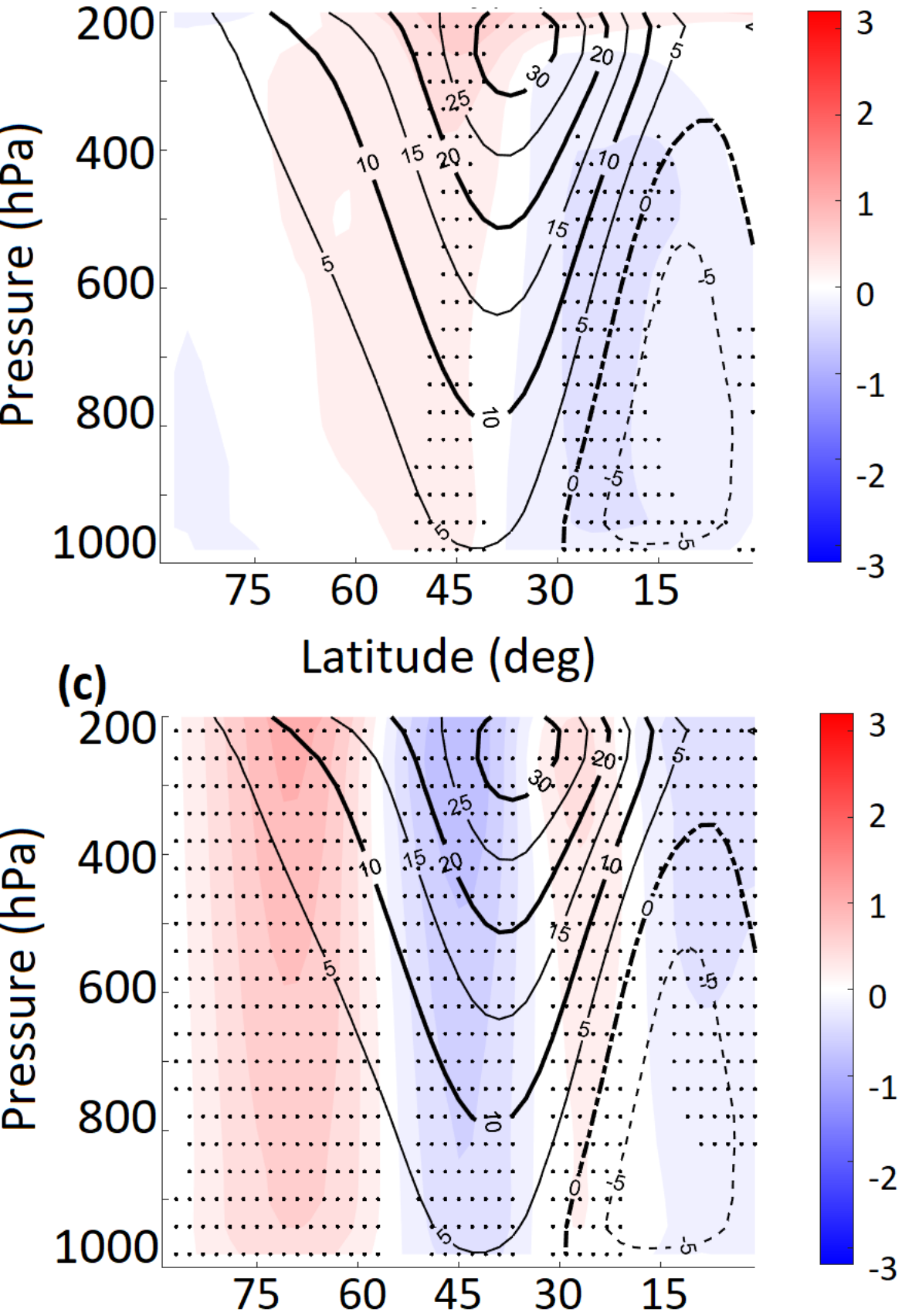
Pressure (hPa)
200
400
600
800
1000
75
60
45
30
15
Latitude (deg)
3
2
1
0
-1
-2
-3

(b)

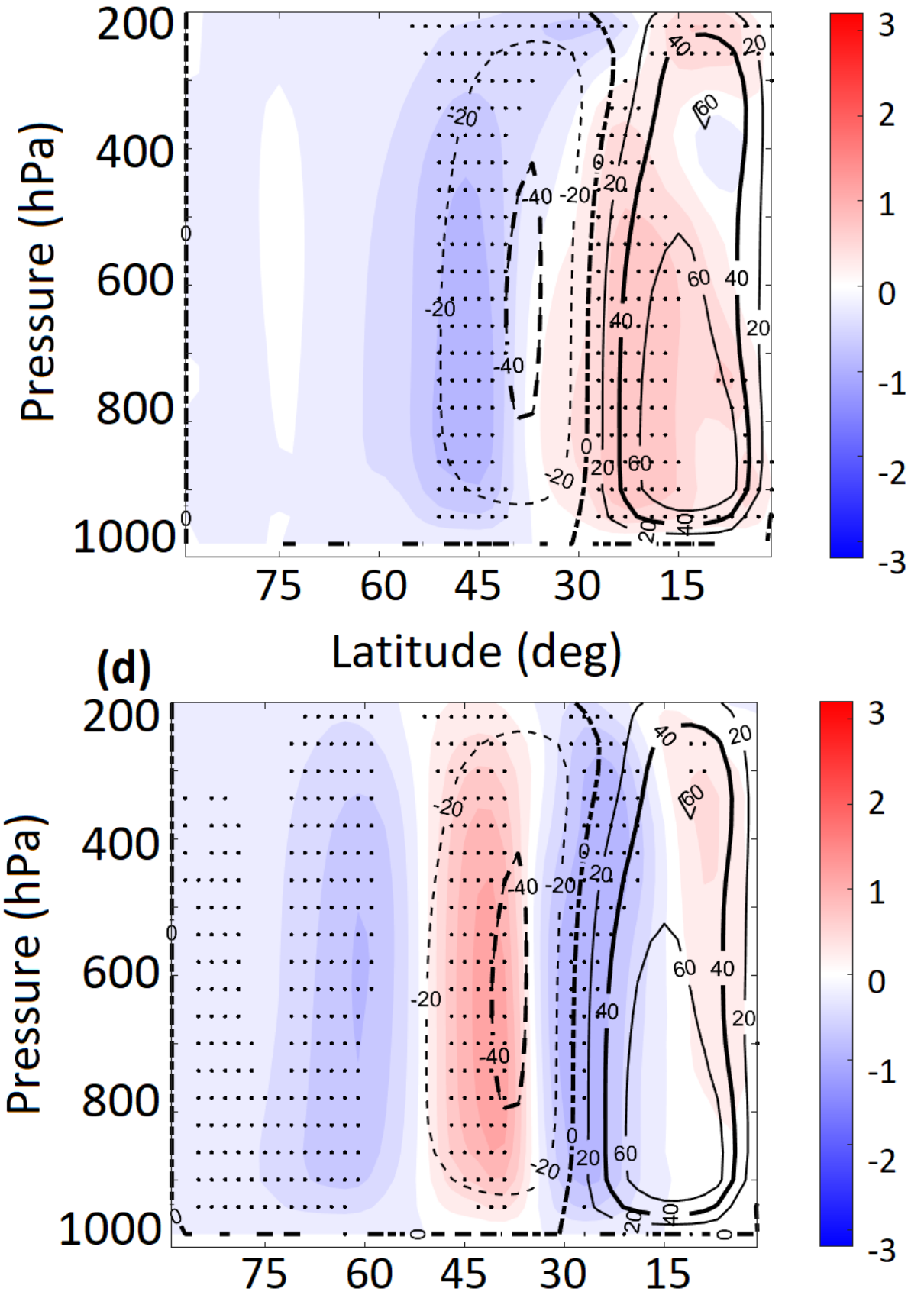
Pressure (hPa)
200
400
600
800
1000
75
60
45
30
15
Latitude (deg)
3
2
1
0
-1
-2
-3

(c)

Pressure (hPa)
200
400
600
800
1000
75
60
45
30
15
Latitude (deg)
3
2
1
0
-1
-2
-3

(d)

Pressure (hPa)
200
400
600
800
1000
75
60
45
30
15
Latitude (deg)
3
2
1
0
-1
-2
-3

(e)

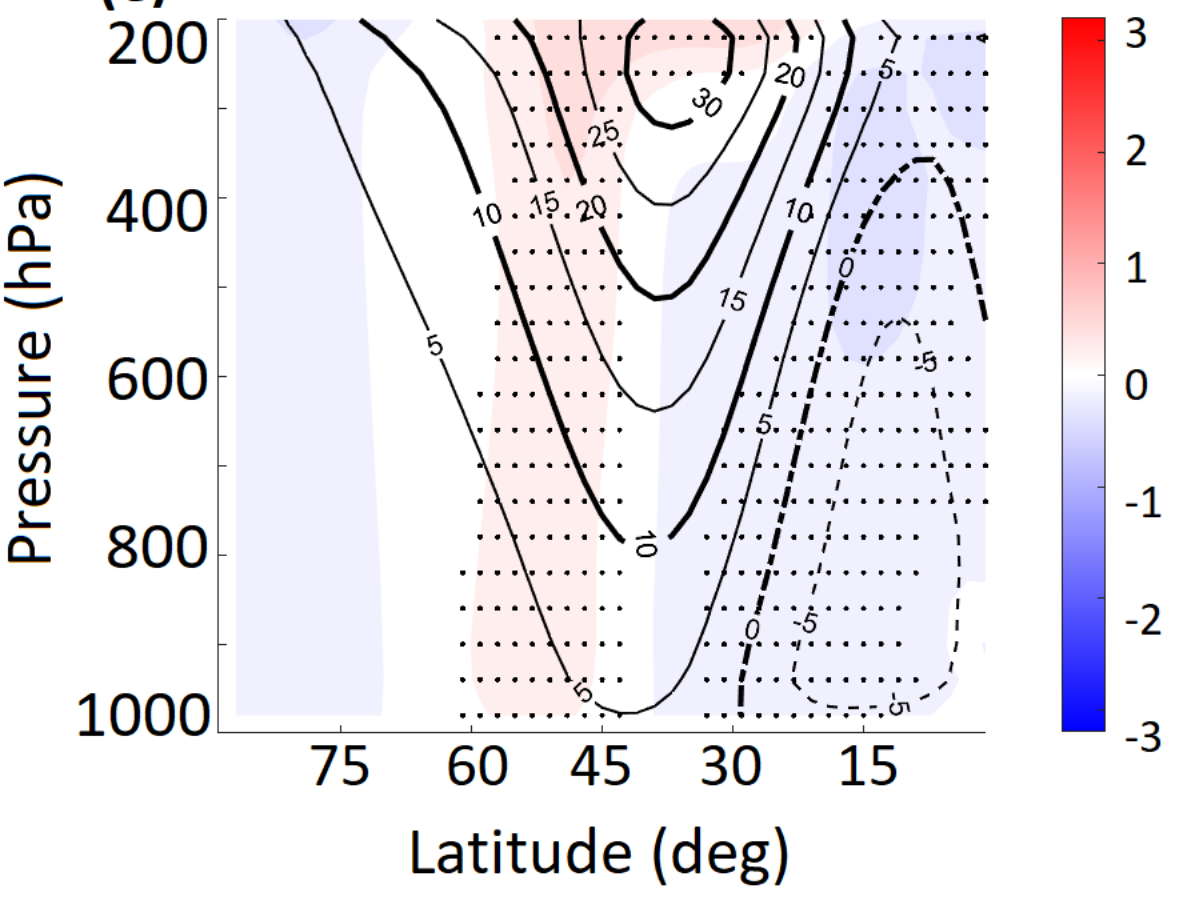
Pressure (hPa)
200
400
600
800
1000
75
60
45
30
15
Latitude (deg)
3
2
1
0
-1
-2
-3

(f)

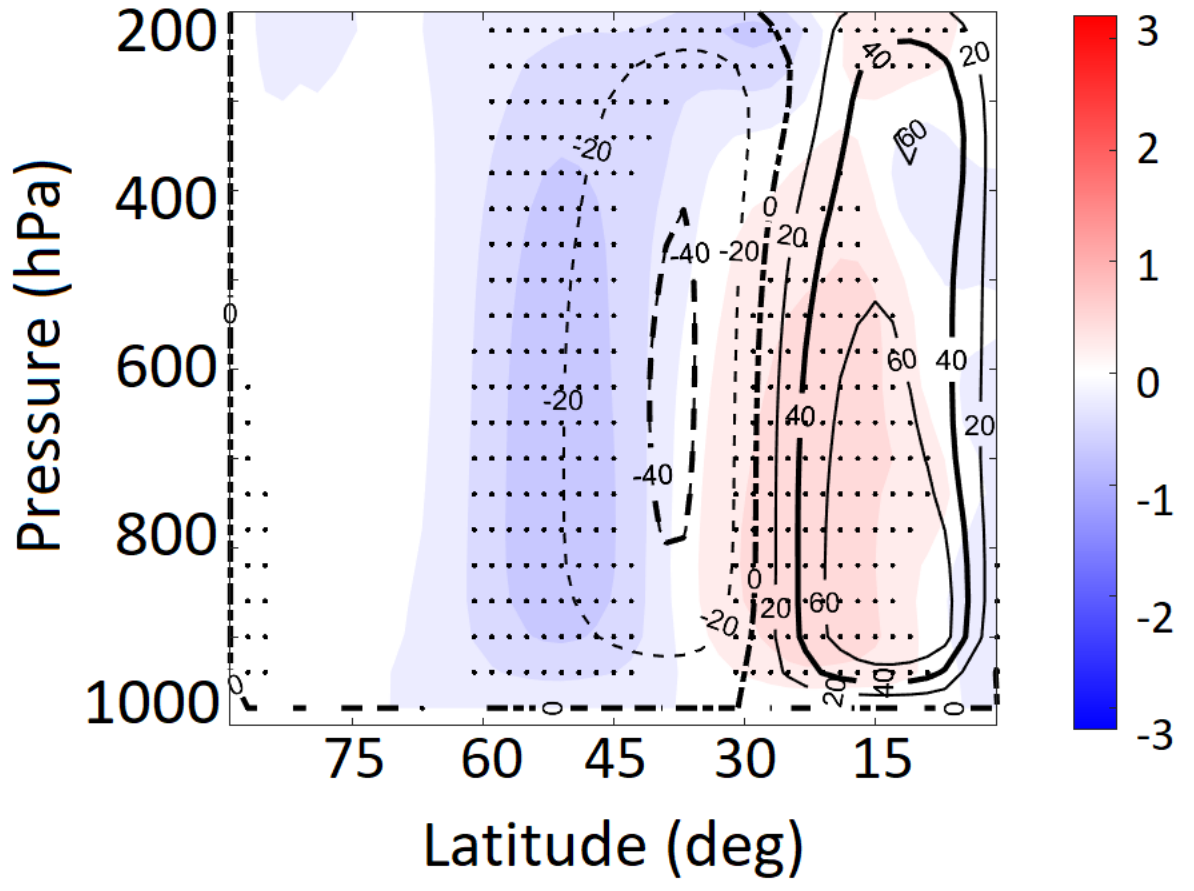
Pressure (hPa)
200
400
600
800
1000
75
60
45
30
15
Latitude (deg)
3
2
1
0
-1
-2
-3

(g)

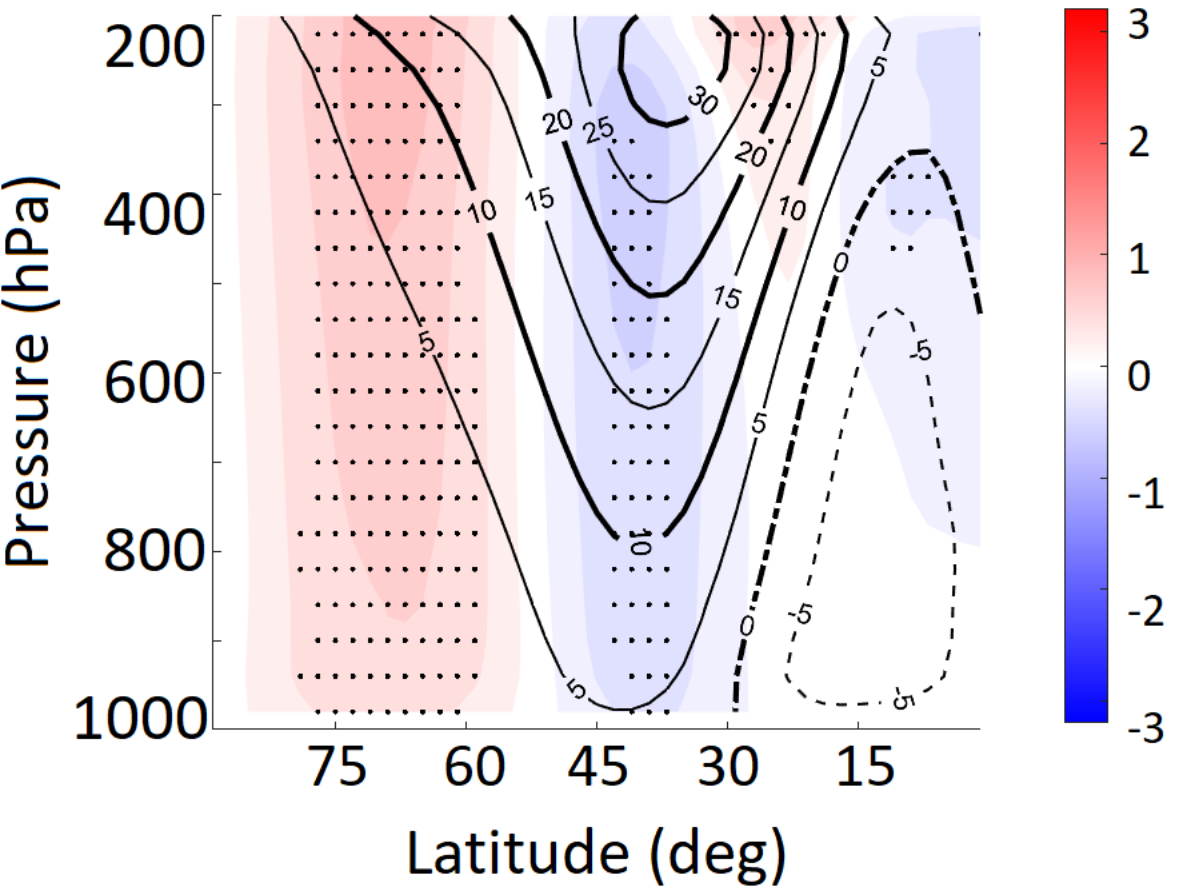
Pressure (hPa)
200
400
600
800
1000
75
60
45
30
15
Latitude (deg)
3
2
1
0
-1
-2
-3

(h)

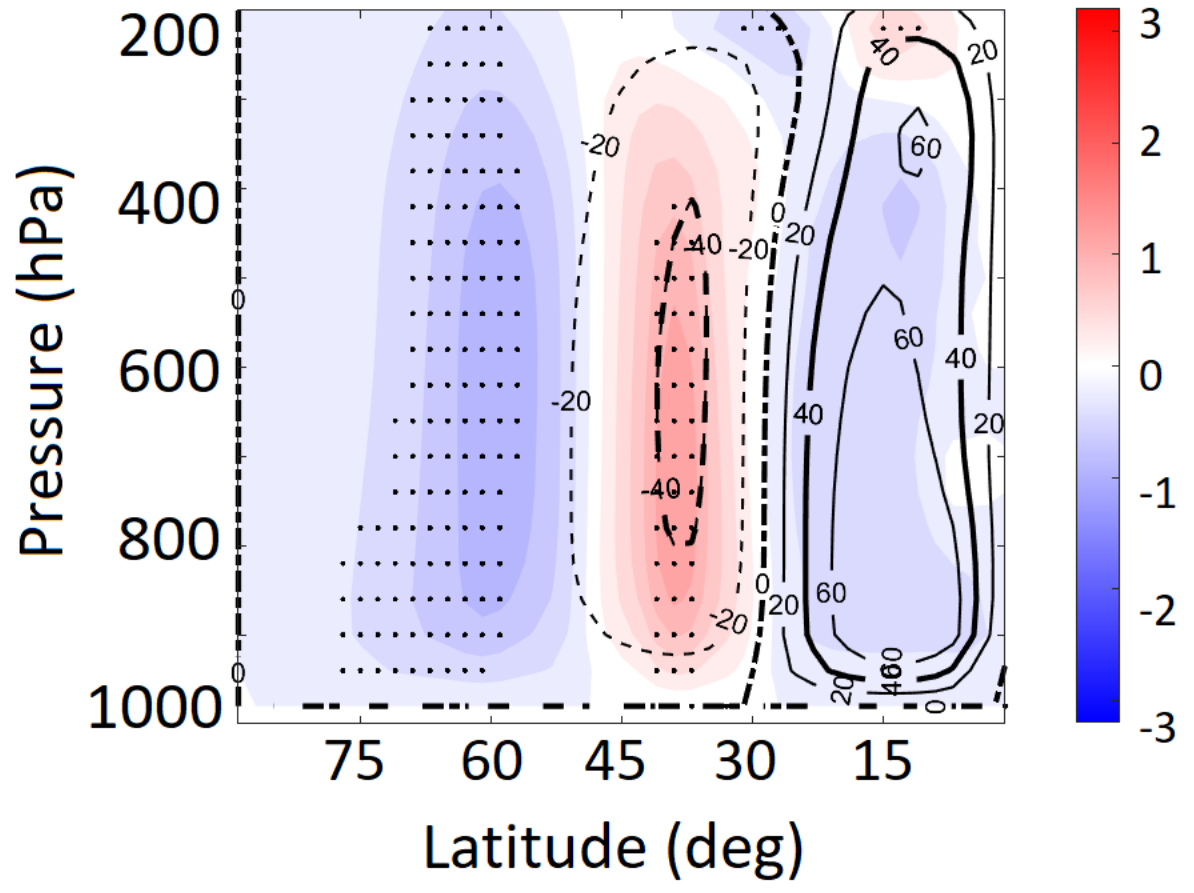
Pressure (hPa)
200
400
600
800
1000
75
60
45
30
15
Latitude (deg)
3
2
1
0
-1
-2
-3

Figure 6.

(a)

Pressure (hPa)

200
400
600
800
1000

75 60 45 30 15

Latitude (deg)

0.8
0.4
0
-0.4
-0.8

(b)

Pressure (hPa)

200
400
600
800
1000

75 60 45 30 15

Latitude (deg)

2.0
1.0
0
-1.0
-2.0

(c)

Pressure (hPa)

200
400
600
800
1000

75 60 45 30 15

Latitude (deg)

2.0
1.0
0
-1.0
-2.0

(d)

Pressure (hPa)

200
400
600
800
1000

75 60 45 30 15

Latitude (deg)

2.0
1.5
1.0
0.5
0
-0.5
-1.0

Figure 7.

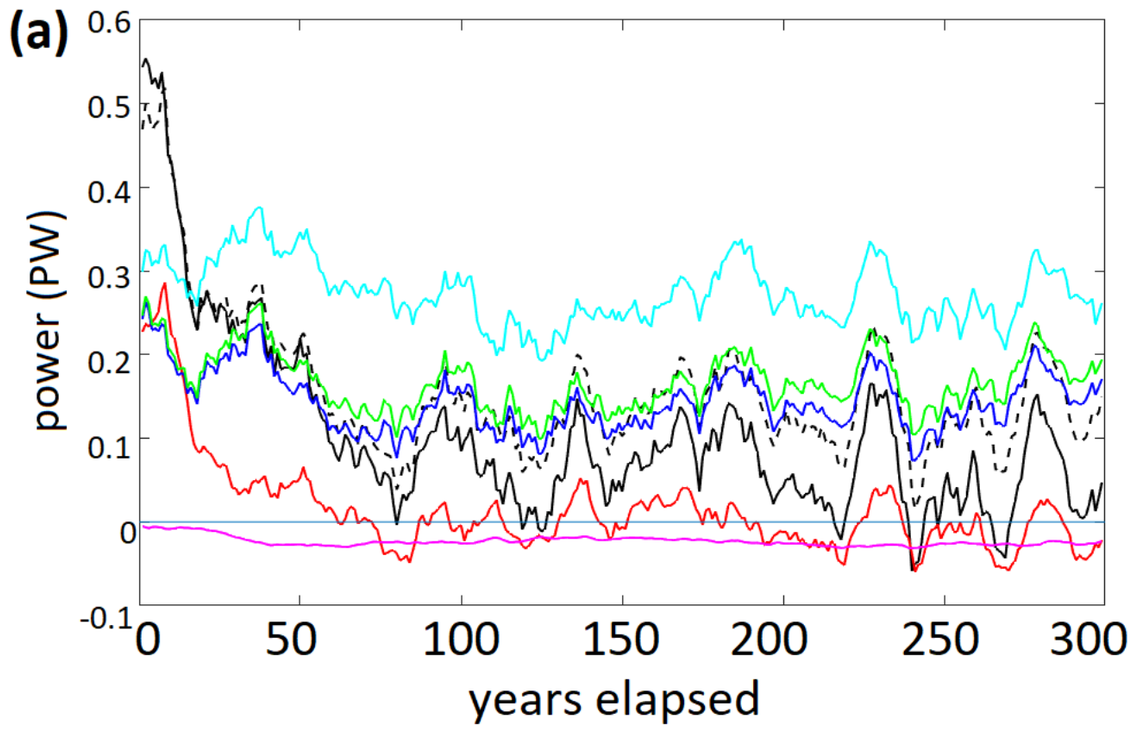
(a)
power (PW)
years elapsed

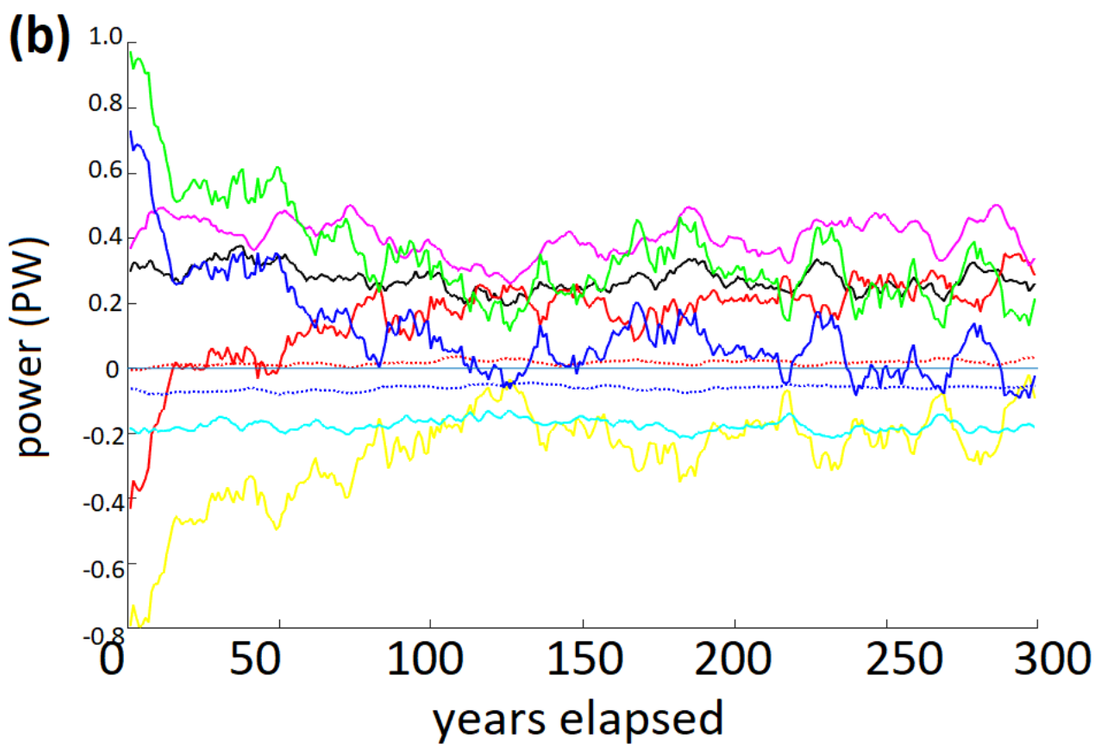
(b)
power (PW)
years elapsed

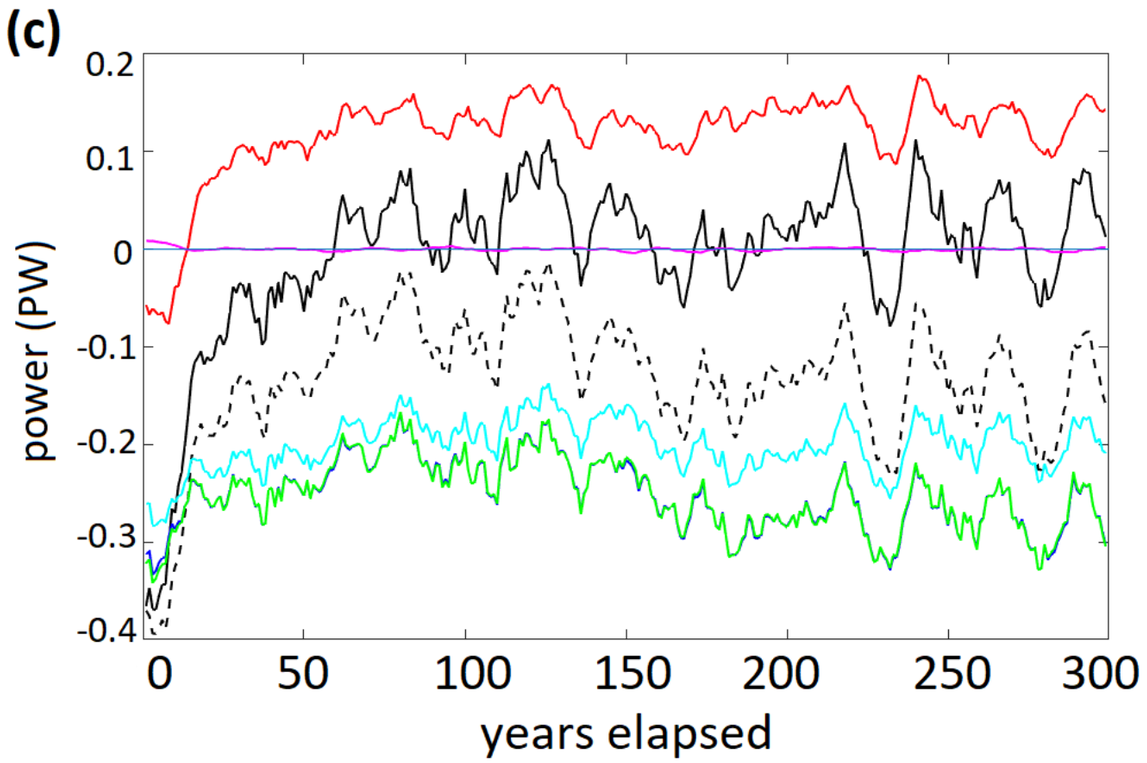
(c)
power (PW)
years elapsed

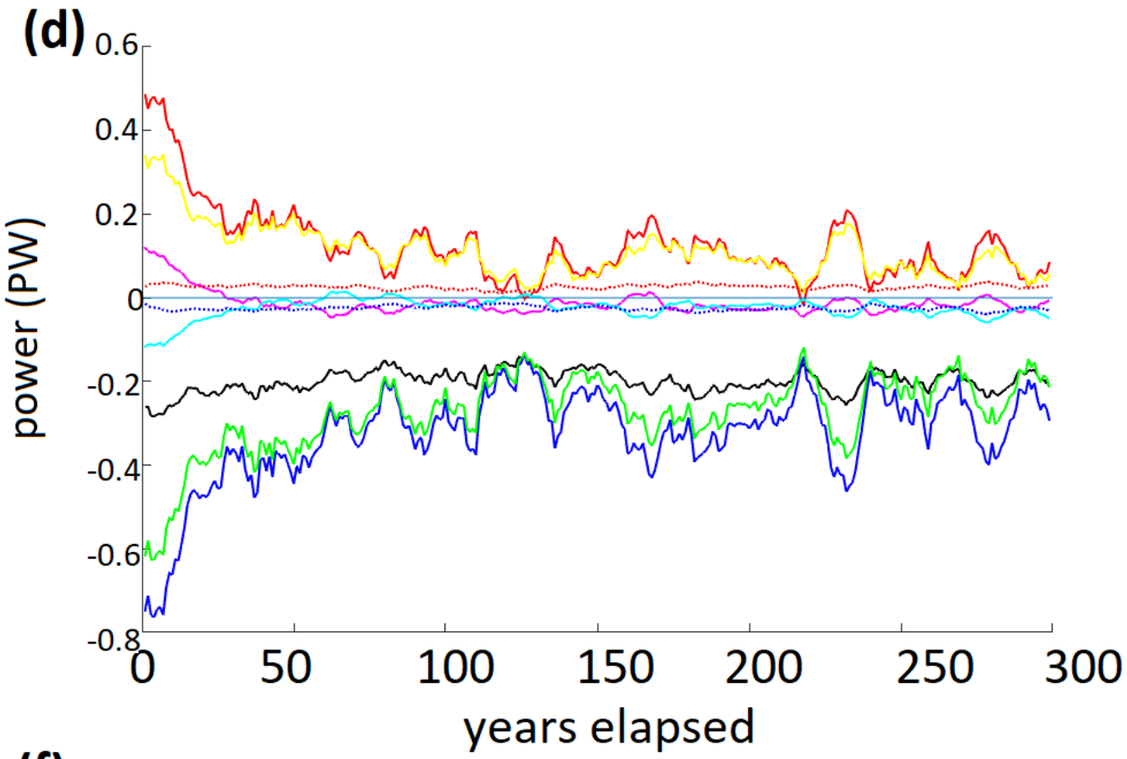
(d)
power (PW)
years elapsed

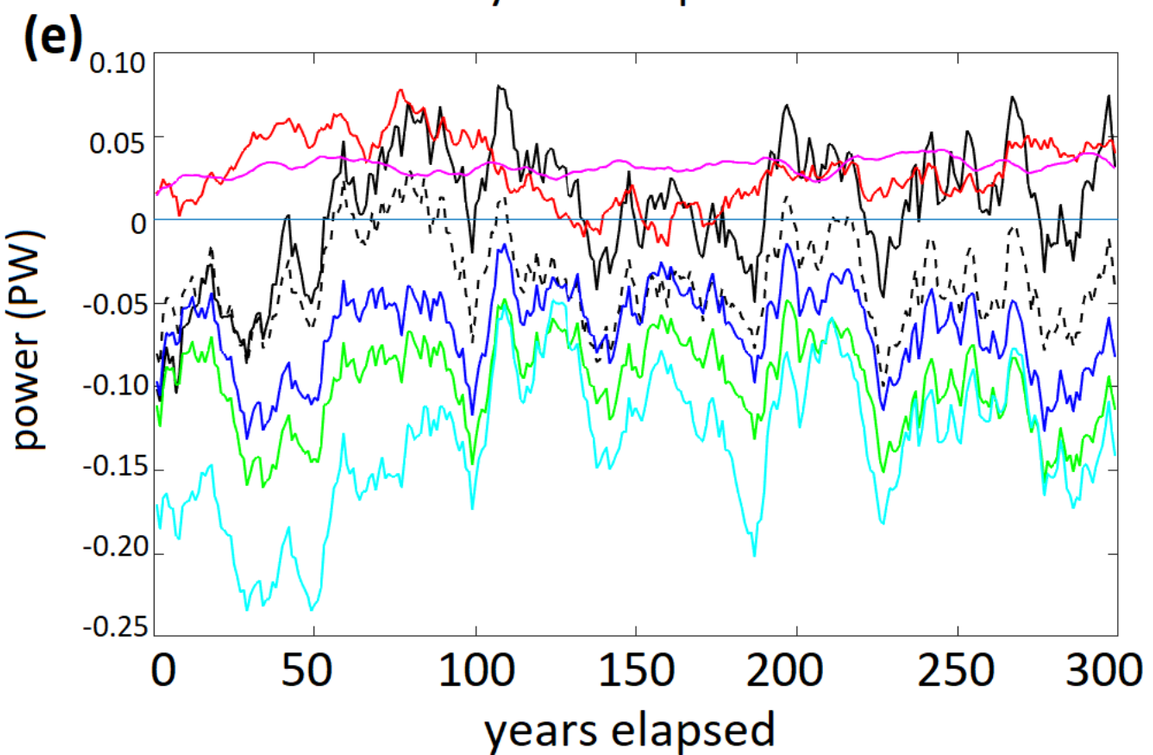
(e)
power (PW)
years elapsed

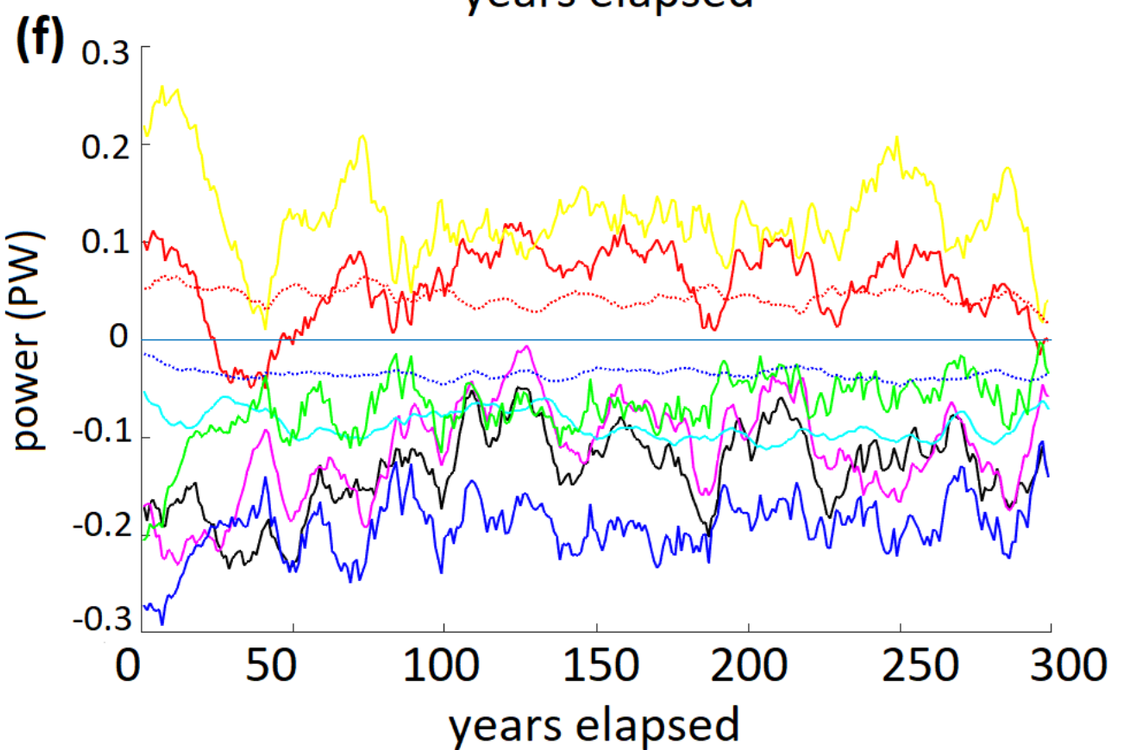
(f)
power (PW)
years elapsed

Figure 8.

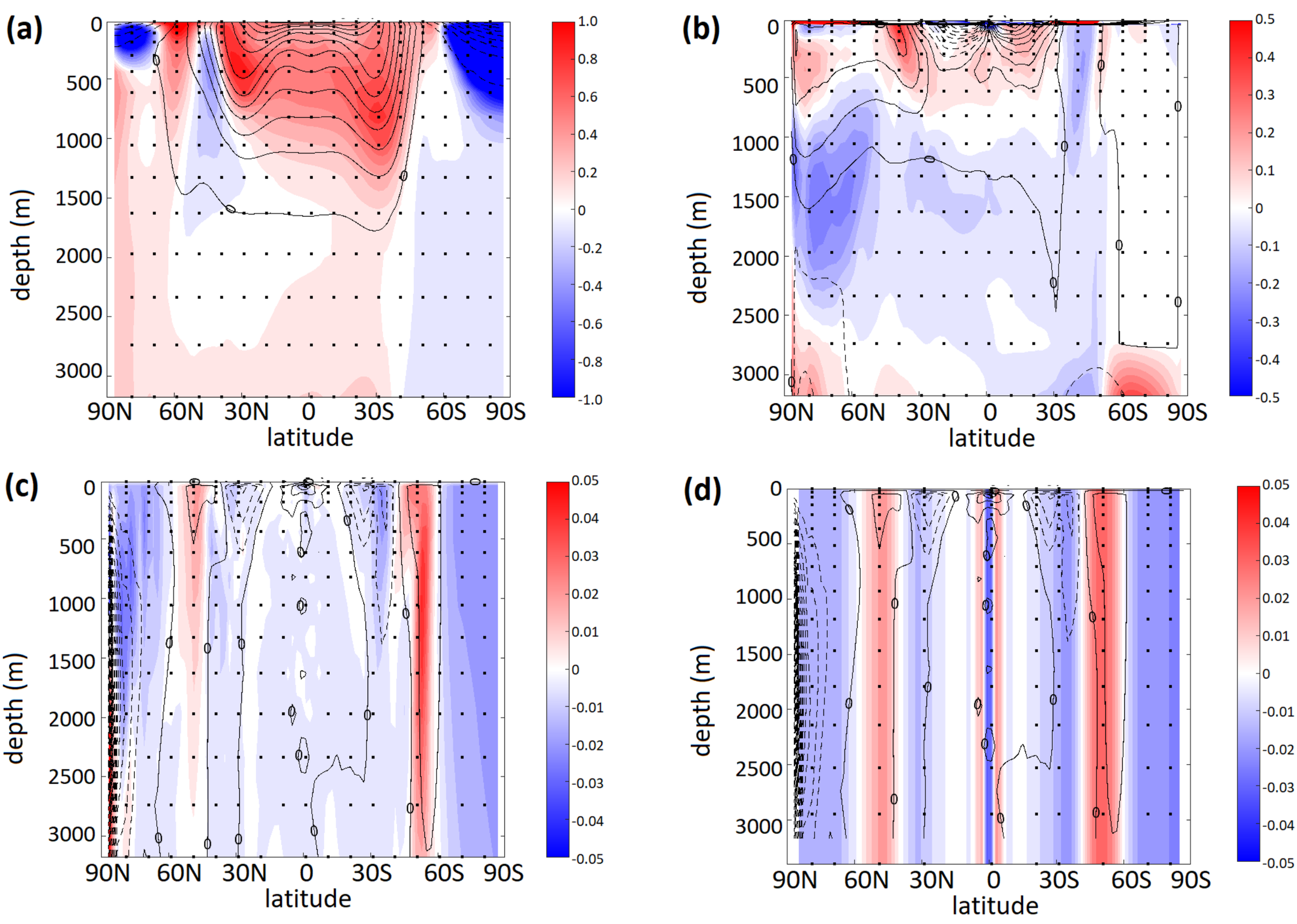
(a)
(b)
(c)
(d)
depth (m)
latitude
0
500
1000
1500
2000
2500
3000
90N
60N
30N
0
30S
60S
90S
1.0
0.8
0.6
0.4
0.2
0
-0.2
-0.4
-0.6
-0.8
-1.0
0.5
0.4
0.3
0.2
0.1
0
-0.1
-0.2
-0.3
-0.4
-0.5
0.05
0.04
0.03
0.02
0.01
0
-0.01
-0.02
-0.03
-0.04
-0.05